12-14-2018

Fatigue Crack Growth Tests and Analyses on a Ti-6Al-4V (STOA) Alloy using the Proposed ASTM Procedures for Threshold Testing

Aniket Chandrakant Mote

Fatigue crack growth tests and analyses on a Ti-6Al-4V (STOA) alloy using the proposed ASTM procedures for threshold testing

By

Aniket Chandrakant Mote

A Thesis
Submitted to the Faculty of
Mississippi State University
in Partial Fulfillment of the Requirements
for the Degree of Master of Science
in Aerospace Engineering
in the Department of Aerospace Engineering

Mississippi State, Mississippi

December 2018

Fatigue crack growth tests and analyses on a Ti-6Al-4V (STOA) alloy using the proposed ASTM procedures for threshold testing

By

Aniket Chandrakant Mote

Approved:

_____

Thomas E. Lacy Jr.
(Major Professor)

_____

James C. Newman Jr.
(Co-Major Professor)

_____

Matthew W. Priddy
(Committee Member)

_____

David S. Thompson
(Graduate Coordinator)

_____

Jason M. Keith
Dean
Bagley College of Engineering

Name: Aniket Chandrakant Mote

Date of Degree: December 14, 2018

Institution: Mississippi State University

Major Field: Aerospace Engineering

Major Professors: Dr. Thomas E. Lacy Jr., Dr. James C. Newman Jr.

Title of Study: Fatigue crack growth tests and analyses on a Ti-6Al-4V (STOA) alloy using the proposed ASTM procedures for threshold testing

Pages in Study 63

Candidate for Degree of Master of Science

This thesis investigates fatigue crack growth rate behavior in the threshold and near-threshold regimes for a Ti-6Al-4V (STOA) alloy using two proposed ASTM procedures- (1) load-shedding (LS) using a larger load-shed rate than the current ASTM Standard E647 load-reduction (LR) test procedure, and (2) compression pre-cracking constant-amplitude (CPCA) or load-increasing (CPLI) and load-shedding (CPLS). Tests were conducted at a low stress ratio (R = 0.1) on compact C(T) specimens of two different widths (W = 51 and 76 mm) and threshold fatigue crack growth rates were generated. These test data were compared to previous test data produced from the same batch of material using the current LR and the CPCA test procedure.

While no test procedure provided an exact representation of the threshold value (ΔK_{th}), the compression pre-cracking (CP) procedures were the most promising. The LR, LS, and CPLS test procedures were influenced by prior loading-history and various crack-closure mechanisms, leading to higher ΔK_{th} values and slower crack growths in the threshold regime. The LS tests (at shed-rates of -0.08,

-0.32, and -0.95 mm^{-1}) generated ΔK_{th} values that were 15% to 32% higher than the estimated threshold stress-intensity factor range $(\Delta^* K_{th})_{R=0.1}$. The CP test procedures are a more accurate alternative for developing near-threshold and threshold fatigue crack growth rates. The CPLS test procedure produced a ΔK_{th} value that was 10% higher than $(\Delta^* K_{th})_{R=0.1}$. LR and LS tests produced different ΔK_{th} values as a function of the specimen width for the given load ratio. The CP test procedures produced consistent crack growth rates over the same range of ΔK values examined, independent of the specimen width. Further research is required for developing test procedure(s) capable of providing a more definitive representation of the ΔK_{th} value and closure-free fatigue crack growth rates in the threshold regime.

DEDICATION

This work is dedicated to the most important women in my life- my grandmother, Sindhu Chavan, and my mother, Dr. Pournima Mote. Their infinite love, guidance, and encouragement helped me be become the person I am today.

ACKNOWLEDGEMENTS

अज्ञानतिमिरान्धस्य ज्ञानाञ्जनशलाकया | [redacted]
चक्षुरून्मीलितं येन तस्मै श्रीगुरवे नमः ||
[redacted] (स्कंदपुराण:उत्तरखंड:गुरूगीता: ३४)

I would like to thank the "Superstar of Modern Aeronautics", Dr. James C. Newman Jr., without whom this work could not have been accomplished. It was a great joy and a real privilege to work with Dr. Newman and learn some critical skills of experimental fatigue testing. Dr. Newman's kid-like enthusiasm and curiosity towards the field of fatigue and fracture is simulating and infectious.

I want to express my sincere gratitude towards my major professor, Dr. Thomas E. Lacy Jr. Dr. Lacy resurrected me off a sinking ship of obliviousness and bewilderment. He continues to tirelessly mentor and challenge the best in of me.

I would also like to thank Dr. Matthew W. Priddy, for agreeing to serve on my committee and being patient with me. Dr. Priddy was always gregarious and approachable whenever I needed him.

I want to take this opportunity to recognize my dear friends, Dr. Kalyan Raj Kota and Nimesh Jayakody, for their steadfast support and constructive critique, that has helped me immensely to leap through many graduate life hurdles.

I also want to thank my extended family and team at Computer-Based Testing. Thank you, Ms. Mary Vaughn, for always being supportive and for funding a major part of my graduate studies.

To my friends Nikhil, Randika, Shubham, Gaurav, Saurabh, Ajinkya, Shashank and Yashaswin- thank for tolerating me and for making Starkville home away from home.

A special shout out and a big thank you to Paul McGarry. I cannot imagine myself at Mississippi State University without Paul's endless support and push throughout my graduate and professional careers.

Finally, to my family- thank you for backing my endeavors and for everything you do for me. I hope this makes you proud! I love you all 😘.

On to the next thing here I go!!!

TABLE OF CONTENTS

LIST OF TABLES

LIST OF FIGURES

NOMENCLATURE

Symbols:

B	Specimen thickness, mm.
a	Crack length, mm.
a_n	Crack-starter notch length, mm.
C	Normalized K-gradient (or load-shed rate), mm^{-1}.
da/dN	Crack growth rate, m/cycle.
E	Modulus of elasticity, GPa.
E_A	Reference modulus of elasticity, 70 GPa.
h	Notch height, mm.
K_c	Critical stress-intensity factor at failure, MPa-√m.
K_{cp}	Minimum stress-intensity factor during compression pre-cracking, MPa-√m.
K_{CT}	Stress-intensity factor for compact specimen under tensile loading, MPa-√m.
K_{max}	Maximum stress-intensity factor, MPa-√m.
$K_{max,i}$	Maximum applied K_{max} at the end of fatigue pre-cracking procedure prior to performing a K-decreasing test procedure, MPa-√m.
K_{min}	Minimum stress-intensity factor, MPa-√m.
K_{op}	Stress-intensity factor corresponding to crack-opening load, MPa-√m.
N	Number of cycles.
P_{alt}	Alternating load, $(P_{max} - P_{min})/2$, lbs.
P_{max}	Maximum applied load, lbs.

$P_{max, i}$	Maximum applied load at the beginning of the test, lbs.
P_{min}	Minimum applied load, lbs.
P_{mean}	Mean load, $(P_{max} + P_{min})/2$, lbs.
P_o	Crack-opening load.
P_{oR}	Crack-opening load ratio.
R	Load (P_{min}/P_{max}) ratio or stress ratio.
r_{cp}	Plastic-zone size during compression pre-cracking, mm.
W	Specimen width, mm.
Δa	Crack extension, mm.
ΔK	Stress-intensity factor range, MPa-$\sqrt{m}$.
ΔK_{eff}	Effective stress-intensity factor range, MPa-$\sqrt{m}$.
ΔK_i	Initial stress-intensity factor range, MPa-$\sqrt{m}$.
ΔK_{th}	Fatigue crack growth threshold stress-intensity factory range, MPa-$\sqrt{m}$.
$(\Delta K_i)_R$	Initial stress-intensity factor after compression pre-cracking, MPa-$\sqrt{m}$.
$(\Delta K_{th})_7$	Threshold stress-intensity factor at R = 0.7, MPa-$\sqrt{m}$.
$(\Delta^* K_{th})_R$	Estimated threshold stress-intensity factor at R, MPa-$\sqrt{m}$.
α	Constraint factor.
σ_o	Flow stress (average of yield and ultimate tensile strength), MPa.
σ_u	Ultimate tensile strength, MPa.
σ_{ys}	Yield stress (0.2% offset), MPa.

Abbreviations:

AMS	Aerospace Material Specification.
ASTM	American Society for Testing and Materials.
BFS	Back-face strain gage.
COD	Crack-opening displacement.
CTOD	Crack-tip opening displacement.
CP	Compression pre-cracking test procedures.
CPCA	Compression pre-cracking constant-amplitude test procedure.
CPLI	Compression pre-cracking load-increasing test procedure.
CPLS	Compression pre-cracking load-shedding test procedure.
C (T)	Compact specimen, a single edge-notch specimen loaded in tension.
DICC	Debris-induced crack closure.
NASA	National Aeronautics and Space Administration.
LI	Load-increasing (K or ΔK-increasing, constant R) test procedure.
LR	Current ASTM Standard E647 load-reduction (K or ΔK-decreasing, constant R) test procedure.
LS	Proposed load-shedding test procedure.
OP*X*	Crack-opening load (P_o/P_{max}) ratio at *X*% compliance offset.
PICC	Plasticity-induced crack closure.
RICC	Roughness-induced crack closure.
STOA	Solution treated and overaged.

CHAPTER I

INTRODUCTION

Structural components may experience in-service fatigue damage under cyclic loading conditions. The damage, typically in form of cracking, may emanate and grow from structural flaws or material metallurgical features. Such an accruing fatigue crack growth exceeding a critical crack length can lead to a catastrophic structural failure.

To study the fatigue crack growth in engineering materials, the concept of linear-elastic fracture mechanics (LEFM) developed by Irwin [1] and Paris et al. [2] is used. Fatigue crack growth behavior of metallic materials is classically evaluated using crack growth relationships in terms of a range of crack-tip stress-intensity factor, ΔK, and crack growth rate, da/dN (a = crack length, N = cycle count), at a given load ratio (R = ratio of minimum to maximum load) [3]. Figure 1.1 represents a plot of typical fatigue crack growth rate data for a metallic material at constant load ratio, where fatigue crack growth rate, $\log (da/dN)$, is plotted against $\log (\Delta K)$. The fatigue crack growth curve can be categorized in three distinct regimes: the threshold regime (I), the Paris regime (II), and the fracture regime (III).

In region I (Figure 1.1), as ΔK decreases, the fatigue crack growth slows down drastically leading to a non-linear relationship between ΔK and da/dN [4]. A fatigue

crack growth threshold stress-intensity factor range, ΔK_{th}, an asymptotic value of ΔK at which da/dN approaches zero [5], can be determined in region I. Hence, the region I defining crack growth as either very slow or nonexistent is called as the threshold regime.

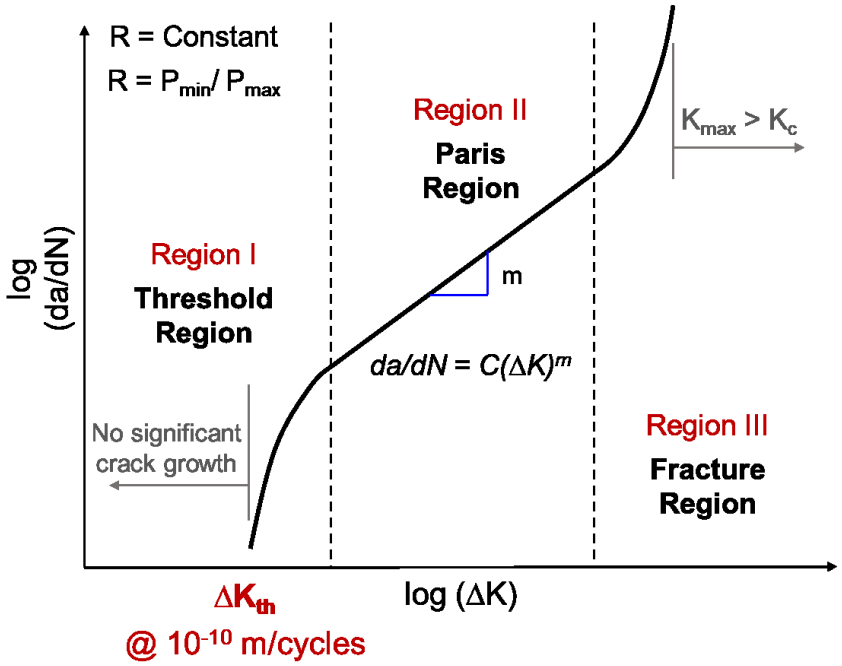

Figure 1.1 Schematic of typical fatigue crack growth rate behavior.

Region II (Figure 1.1), shows a nearly linear relationship between ΔK and da/dN [3] for many materials on log-log plots. As the crack grows towards a critical crack length in region III, ΔK increases and an unstable crack growth is expected. Thus, the relationship between ΔK and da/dN becomes non-linear in region III [6].

A greater part of the fatigue life in a structural component is spent in the region I threshold conditions, whereas region II and III commonly consume smaller portions of the total fatigue life. Traditionally, ΔK_{th} is used as a limit for damage tolerant design [7]. Hence, an accurate determination of ΔK_{th} has a great bearing on

the design of a high strength-high cycle fatigue structure and is also vital for successful crack growth prediction. A structure designed with an inadvertently high ΔK_{th}, may catastrophically fail long before its projected service life. On the contrary, if ΔK_{th} is too low, the structure would have to endure a higher weight penalty.

Figure 1.2 represents experimental fatigue crack growth rate test data for the titanium alloy, Ti-6Al-4V (STOA), at a wide range of load ratios, R, of 0.1, 0.3, 0.5, and 0.8, from threshold to near fracture [8]. It can be observed that for the same ΔK, a faster fatigue crack growth rate is obtained at the higher stress ratio. The fatigue crack growth thresholds (ΔK_{th} at 10^{-10} m/cycle) vary with the given load ratio. In addition, the spread in ΔK at low rates is more than at higher rates.

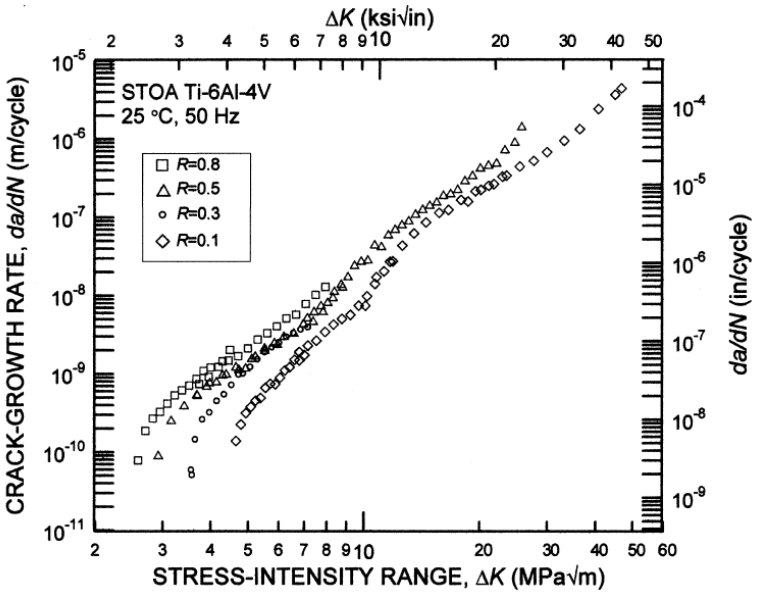

Figure 1.2 Fatigue crack growth data for a Ti-6Al-4V (STOA) alloy at various load ratios [8]

Elber [9] proposed the concept of fatigue crack closure to help understand the load ratio effects on the fatigue crack growth rate behavior. During experiments on

2024-T3 aluminum sheet, Elber recognized an occurrence of a premature crack surface contact under cyclic tensile unloading conditions- before the minimum load [10]. Such behavior was attributed to the residual plastic deformations of the material left behind in the wake of advancing crack. On subsequent cyclic tensile loading, the crack surface is fully open when the crack-opening load occurs. It is generally accepted that there is no crack-tip damage below the crack-opening load, thus the load cycle below the crack-opening load does not contribute to fatigue crack growth. Further, Elber related the fatigue crack growth rate to an effective stress-intensity range, ΔK_{eff}, defined as $\Delta K_{eff} = K_{max} - K_{op}$, where K_{max} is the maximum stress-intensity factor range and K_{op} is the stress-intensity factor corresponding to crack opening load.

The plastic strain field generated at the crack tip, Figure 1.3 [11], modifies the stress-intensity factor range causing crack closure (later termed as plasticity induced crack closure or PICC [12]). The PICC mechanism has hence been used to explain the load ratio dependency [10, 12], near-threshold effects (low ΔK crack growth), and the influence of load-history [13] on the fatigue crack growth rate behavior.

While the past research has demonstrated that PICC is the most dominant and well perceived closure mechanism in metals, existence of the roughness induced crack closure (RICC) [14, 15] and oxide/fretting debris induced crack closure (DICC) [14, 16] mechanisms are suspected under threshold conditions where crack opening displacements are small and crack paths become more torturous [17].

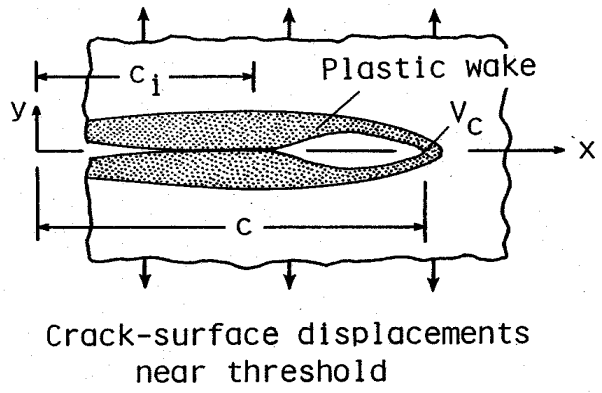

Figure 1.3 A schematic of the plasticity induced crack closure and crack-surface displacements near-threshold crack growth rate behavior [11]

RICC [15, 18] occurs during the cyclic tensile unloading, when rough crack surfaces come in contact. Rough fatigue cracks cause a mixed mode crack tip stress field due to misalignment and displacement of crack surfaces, thus reducing the crack tip driving force. RICC maybe of most significance at low ΔK due to torturous crack growth, small crack tip opening displacements (CTOD) and smaller PICC effect.

Oxidation due to environmental effects and continuous pile-up of fretting debris due to premature crack surface contacts through PICC or RICC, congest the crack surfaces [14, 16, 18]. As the crack tip advances, oxidation occurs as soon as the newly created crack surfaces are exposed to environmental agents. For high K_{max} tests or where CTOD is large, oxide debris may not cause a substantial crack closure. However, oxide/fretting DICC may have significant effects near-threshold, where the CTOD is small, with rough crack surfaces [19].

It is evident from the earlier research [11, 19, 20] that crack closure may be observed far behind the crack tip, and not just near the crack-tip. In Figure 1.4 [19],

remote closure occurring during constant R load-reduction threshold testing is shown. Crack contact occurs in the crack wake due to large amount of plasticity created by higher loads during the early constant-amplitude loading (higher stress-intensity factor) sequence, while the crack-tip (feeling smaller stress-intensity factors) remains open. Such remote crack closure caused due the load-history effects, has been recognized to significantly affect the crack-tip stress-strain field.

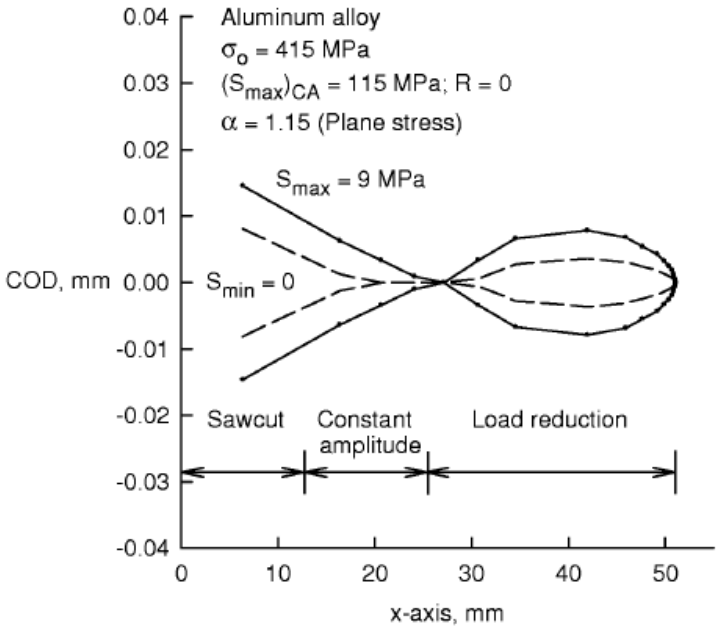

Figure 1.4 Remote crack closure indicated by the crack opening displacement (COD) due to load-history effects [19]

CHAPTER II

RESEARCH MOTIVATION AND OBJECTIVES

A large portion of fatigue life for high-cycle aerospace and machinery components is often spent in the threshold region. Traditionally ΔK_{th} is used as a limit for damage tolerant design [7]. Past research has established that the threshold and near-threshold region of the crack growth rate curve is vital for a successful prediction of the service life and for determining proper inspection intervals, mainly for cracks originating from very small initial discontinuities [21].

At present, the threshold fatigue crack growth regime is experimentally defined using a load-reduction (LR) test procedure in ASTM Standard E647 [22]. The LR (K-decreasing, constant R) test procedure has been shown to produce higher thresholds and slower rates in the threshold regime than steady-state constant-amplitude data. Tests have shown that the LR test procedure is affected by the loading history, induces remote closure due to plastically deformed material in the wake of crack to prematurely slow down the crack growth [11, 12, 19, 20]. In addition, the LR test procedure produce "fanning" in the threshold region, due to elevated crack closure levels in the low R tests. Thus, the LR test procedure defeats the original intent in ASTM Standard E647, to produce a "steady-state" constant-amplitude data, without any load-history effects

The ASTM Committee E08 on Fatigue and Fracture that regulates the ASTM Standard E647 [22] have proposed two alternate procedures to counter the load-history effects. Revision to the ASTM Standard E647 that includes these proposed procedures is currently under balloting process. These procedures are:

(1) load-shedding (LS) using a larger load-shed rate than the current ASTM Standard E647 LR procedure, and

(2) compression pre-cracking constant-amplitude (CPCA) or load-shedding (CPLS)

To generate fatigue crack growth rate data in the threshold and near-threshold regimes, without appreciable load-history effects, a "compression-compression" pre-cracking procedure is used. The compression pre-cracking (CP) procedure was championed by Newman et al. [23- 32] by conducting near-threshold fatigue crack growth tests on a wide variety of materials. Using the CP procedure, pre-notched fatigue test specimens are cycled under compression-compression loading to produce a very small initial crack, which naturally slows down during fatigue cycling. Then the specimen is subjected to a constant-amplitude loading (CPCA) procedure to generate crack growth rate data in the near-threshold regime; or a load-shedding (CPLS) test to generate very low crack growth rates in the threshold regime at the desired load ratio. For the material of interest in the current study, titanium alloy Ti-6Al-4V (STOA), past tests [27, 32] using the CPCA test procedure have demonstrated lower thresholds than the current ASTM LR test procedure.

The key objective of this study is to determine the fatigue crack growth rates in threshold and near-threshold regimes for the titanium alloy, Ti-6Al-4V (STOA), using the two proposed ASTM test procedures. These experimental test datasets will then be compared with the previous test data [27, 32] produced from the same batch of material using the current LR and the CPCA test procedures.

CHAPTER III

THRESHOLD AND NEAR-THRESHOLD TEST PROCEDURES

The primary objective of a fatigue crack growth rate test is to determine "steady-state" constant-amplitude ΔK-da/dN data at constant stress ratio. The current chapter will present and discuss the following threshold and near-threshold test procedures:

1. Current load-reduction test procedure.
2. Current constant K_{max} test procedure.
3. Proposed load-shedding test procedure.
4. Compression pre-cracking test procedures.

3.1 Current load-reduction test procedure

The LR (K or ΔK-decreasing, constant R) test procedure was developed in early 1970's by Paris et al. [14, 33] to generate data at low values of stress-intensity factor ranges and approaching the threshold conditions. Later, Bucci et al. [5] and Hudak et al. [34] finalized the procedure, which was incorporated into the current ASTM Standard E647 [22]. The LR procedure has since been used to generate threshold fatigue crack growth rate data and determine ΔK_{th}. To help characterize the loading conditions for many structural components, the current LR test procedure reproduces a wide range, i.e., low and high stress ratios of fatigue crack thresholds.

Initial test starting load levels are selected such that the crack growth rates immediately from crack-starter notch are less than 10^{-8} m/cycle. Specimen is fatigue pre-cracked under constant amplitude tensile loading at R equal to or lower than the desired R for the LR test. Once a pre-crack of adequate size is obtained, the LR test is initiated by cycling at a ΔK and K_{max} level equal to or greater than the terminal fatigue pre-cracking values. Subsequently, loads are shed (decreased) as the crack grows, such that the range of stress-intensity factor reduces at an exponential rate, until the lowest ΔK (usually ΔK_{th} 10^{-10} m/cycle) or crack growth rate of interest is obtained. Upon developing rates at or near the target 10^{-10} m/cycle, the test control is changed to constant R load-increasing (ΔK-increasing) loading scheme, to 'trace' back up the crack growth rate curve, to ensure that the LR data and the load-increasing (LI) data are in agreement.

The rate of load shedding is achieved by limiting the normalized K-gradient, C, as:

$$C = \left(\frac{1}{K}\right) \cdot \left(\frac{dK}{da}\right) > -0.08\ mm^{-1}\ (-2\ in^{-1}) \tag{3.1}$$

This is equivalent to a 5% change in stress every 0.5 mm of crack extension. When using an automated technique for load shedding in a continuous manner, the standard allows a normalized K-gradient of -0.2mm^{-1} (-5 in^{-1}), i.e., a 10% change every 0.5 mm of crack extension.

For many years, there has been a concern with the possible load-history effects on the near-threshold fatigue crack growth data, such as elevated thresholds and slower rates than steady-state data [11]. A schematic of typical ΔK-da/dN behavior

from the current ASTM Standard E647 LR test is depicted in Figure 4.1. For the K-decreasing constant R (i.e., LR) test procedure, the standard [22] suggests using pre-cracking crack growth rates equal to or less than 10^{-8} m/cycle (4×10^{-7} in/cycle) to initiate load-shedding. Experimental tests and measurements have demonstrated that the LR test procedure develops crack closure levels above the steady state magnitude [35]. For a LR test with an initial stress-intensity factor range (ΔK_i) level such as ΔK_1, the loads are shed with a decreasing ΔK at constant R, and a threshold $(\Delta K_{th})_1$ may be obtained. If a lower ΔK_i value such as ΔK_2 is used, a lower threshold $(\Delta K_{th})_2$ with faster crack growth rates may be generated. The LR tests may exhibit a phenomenon called "fanning" in the threshold regime with the load ratio, where the spread in ΔK at a low rate is larger than at higher rates as a function of R. The E647 LR procedure considers that the crack tip behavior is totally controlled by ΔK and do not regard the crack closure or the load-history effects.

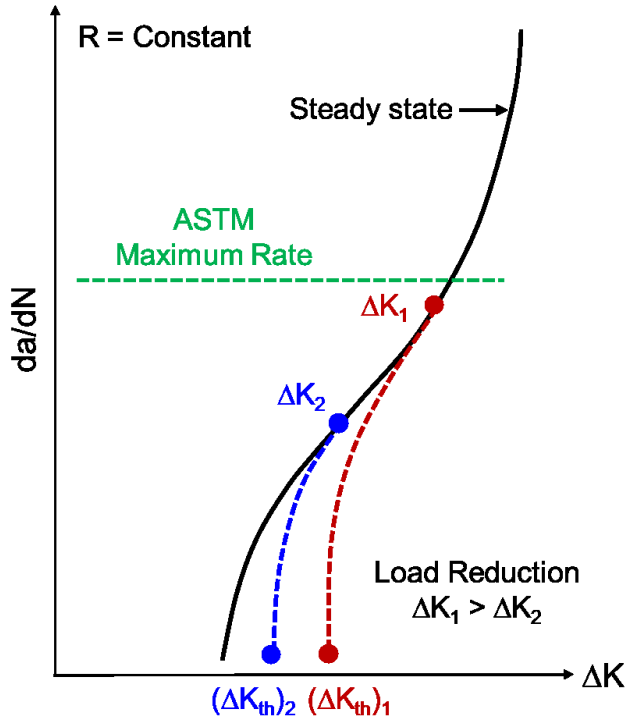

Figure 3.1 Typical near-threshold and threshold fatigue crack growth behavior under load-reduction test procedure.

3.2 Current constant K_{max} test procedure

The K_{max} test procedure was developed by Herman et al. [36]. The test procedure reduces ΔK, by reducing the load amplitude, i.e., raising the K_{min}, while the K_{max} remains constant. The procedure generates low crack growth rates at very small ΔK values, and the stress ratio near and at threshold is generally greater than 0.9.

The constant K_{max} test procedure for obtaining threshold, purportedly develops a threshold that is not influenced by plasticity-induced crack closure [36, 37]. However, the K_{max} test procedure relies on the ΔK-decreasing practice (equation 3.1) to determine threshold, which have shown to introduce load-history

effects. Yamada and Newman [38], using a local strain-gage method demonstrated that the K_{max} test is not completely closure free, and is affected by PICC, RICC and DICC mechanisms. Thus, much more research must be conducted on developing a procedure(s) to generate threshold and near-threshold data that is unaffected by load-history effects.

3.3 Proposed load-shedding test procedure

The new load-shedding procedure, defined in Appendix X5 of the proposed ASTM Standard E647, is similar to the current load-reduction procedure (detailed in section 3.1), except for an alternative load shedding relation that allows higher shed rates. The relationship asserts minimization of the effects of the prior load-history effects by limiting the normalized K gradient parameter (load-shed rate) as follows:

$$C > -0.1\left(\frac{\sigma_{ys}}{K_{max,i}}\right)^2 \tag{3.2}$$

where $K_{max,i}$ is the initial maximum stress-intensity factor at end of the fatigue pre-crack procedure prior to performing a K-decreasing test procedure, and σ_{ys} is the yield strength of the material.

3.4 Compression pre-cracking test procedures

The CP test procedures were developed to generate fatigue crack growth rate data in the threshold and near-threshold regimes, without appreciable load-history effects [27- 32]. A ‘‘compression–compression” pre-cracking procedure, proposed by

Suresh [39], Pippan et al. [40, 41], Forth et al. [25] and Newman et al. [24], is used to determine the steady-state constant-amplitude crack growth rate curve at constant R conditions.

CP test procedures are defined in Appendix X6 of the proposed ASTM Standard E647. The appendix allows two procedures for generating near-threshold and threshold crack growth data. These are (1) compression pre-cracking constant-amplitude (CPCA), and (2) compression pre-cracking load-shedding (CPLS). For the purpose of this study, a third procedure, compression pre-cracking load-increasing (CPLI), was also considered. Figure 3.2 represents typical use of the CP test procedures for generating near-threshold and threshold fatigue crack growth data.

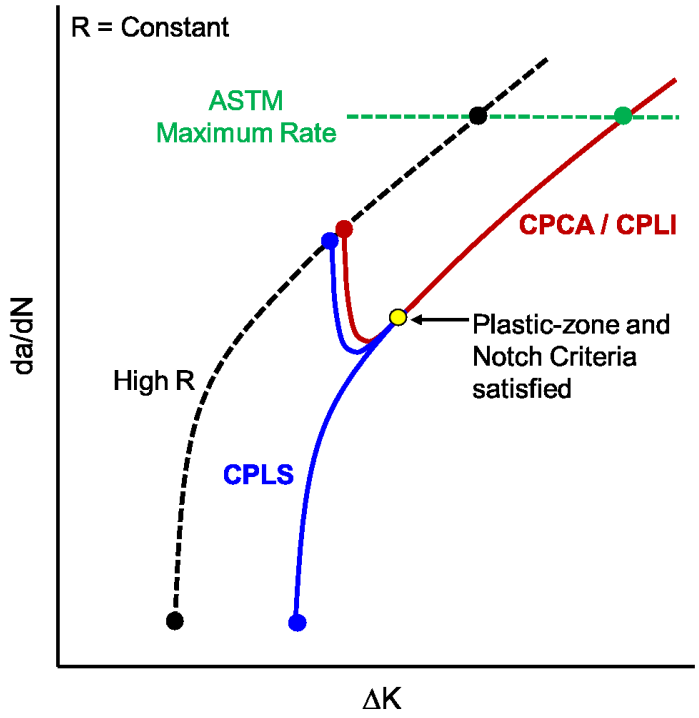

Figure 3.2 Typical fatigue crack growth data using the compression pre-cracking test procedures.

The key difference between the CP test procedure and the ASTM LR or the proposed LS procedure is the fatigue crack initiation methodology. The CP test procedures use cyclic "compression-compression" loading for fatigue pre-cracking, which leave the crack with tensile residual stresses (i.e., open crack at zero load). In contrast, fatigue pre-cracking for the ASTM LR or the proposed LS test procedures is achieved under cyclic tensile loads, which induce compressive residual stresses along the crack front. Further, compression fatigue pre-cracking allows the initial ΔK level for the CP tests to be nearly a factor of two lower, and at a corresponding crack growth rate nearly an order-of-magnitude lower (typically 10^{-9} m/cycle), than the ASTM LR or the proposed LS procedure (typically 10^{-8} m/cycle).

In the CPCA test procedure, after fatigue crack initiation under cyclic compressive loading, the near-threshold fatigue crack growth rate data is generated under constant-amplitude loading. Crack growth rate data is valid once the crack has extended beyond the crack-starter notch effects and away from the tensile residual stresses per the crack-extension criterion (discussed further in this section). The CPLI test procedure exactly similar to the CPCA test procedure, except that the near-threshold fatigue crack growth data is generated under a load-increasing (ΔK-increasing, constant R) loading scheme.

In the CPLS test procedure, after the fatigue crack initiation under cyclic compressive loading, a constant-amplitude loading is used to extend the crack using a crack-extension criterion (discussed further in this section). Once, the crack has grown beyond the crack-extension criteria, a standard ASTM LR (ΔK-decreasing,

constant R) test procedure is used to generate threshold fatigue crack growth rate data.

Fatigue pre-cracking is achieved by cycling a pre-notched specimen under compression-compression loading for 30,000 to 50,000 cycles. The initiated crack naturally stops growing once the threshold is reached under the compression-compression loading, if a large number of cycles were applied.

For the pin loaded C(T) specimens used herein, the compressive stress-intensity factor, $|K_{cp}|$ was determined as:

$$|K_{cp}| = [1 + 2.5\,(1 - \frac{a_i}{W})^{10}]\,K_{CT} \tag{3.3}$$

where K_{CT} is the standard stress-intensity factor (i.e. equation 3.4 below) for the compact specimen under tensile loading.

$$K_{CT} = \frac{P}{B\sqrt{W}} \frac{(2+\alpha)}{(1-\alpha)^{3/2}} (0 \cdot 886 + 4 \cdot 64\alpha - 13.32\alpha^2 + 14 \cdot 72\alpha^3 - 5 \cdot 64\alpha^4) \tag{3.4}$$

where α = a/W, the crack length to width ratio. The minimum compressive stress-intensity factor should be within:

$$0.00015 \leq \frac{|K_{CP}|}{E} \leq 0.0003\,\sqrt{m} \tag{3.5}$$

where E is the modulus of elasticity of the material.

Compression pre-cracking leaves the crack with a negative crack-opening load (i.e., open crack at zero load), before primary fatigue tensile loading. Hence, to overcome the influence of the tensile residual stresses at the crack front and the notch effects on the fatigue crack growth rates, the crack is grown (Δa) under constant-amplitude loading per the crack extension criterion:

$$\Delta a = 4(1 - R)\, r_{CP} \sqrt{\frac{E_A}{E}} \tag{3.6}$$

or

$$\Delta a = h_n \tag{3.7}$$

whichever is larger. Here E is modulus of the material tested, E_A = 70 GPa (10,150 ksi), Δa is crack extension from the notch tip, R is the applied load ratio of the test, $r_{cp} = (|K_{cp}|/\sigma_{FS})^2/\pi$ is an estimate of the plane-stress compression plastic-zone size, and σ_{FS} is the material flow strength (average between yield and ultimate tensile strength).

Initially, a test at nominally closure free stress ratio (R = 0.7) is performed using the LR test procedure (detailed in section 3.1) with a typical K-gradient (i.e. load-shed rate), C ≥ -0.08mm^{-1} (-2 in^{-1}). The threshold $(\Delta K_{th})_7$ established for the R = 0.7 test is then used to estimate the starting conditions for the other stress ratios using simple set of equations and as shown in Figure 3.3. The estimated threshold value, $(\Delta K^*_{th})_R$, at the specified load ratio, R, is calculated as:

$$(\Delta K^*_{th})_R = (\Delta K_{th})_7 \frac{(1-R)}{(1-P_{oR})} \tag{3.8}$$

where, the crack-opening load ratio for R ≥ 0 is

$$P_{oR} = 0.3513 + 0.0303\, R + 0.8607\, R^2 - 0.2672\, R^3 \tag{3.9}$$

The initial stress-intensity factor range $(\Delta K_i)_R$ at the required load ratio, R, is given by:

$$(\Delta K_i)_R = 1.3\, (\Delta K^*_{th})_R \tag{3.10}$$

Post compression pre-cracking, loads are carefully selected to match the $(\Delta K_i)_R$ value. While holding loads constant, the specimen is subjected to a constant-amplitude loading while the crack-extension criteria (i.e., equation 3.6 or 3.7) is satisfied. Further, based on the desired data required, CPLR/CPCA/CPLI tests are conducted.

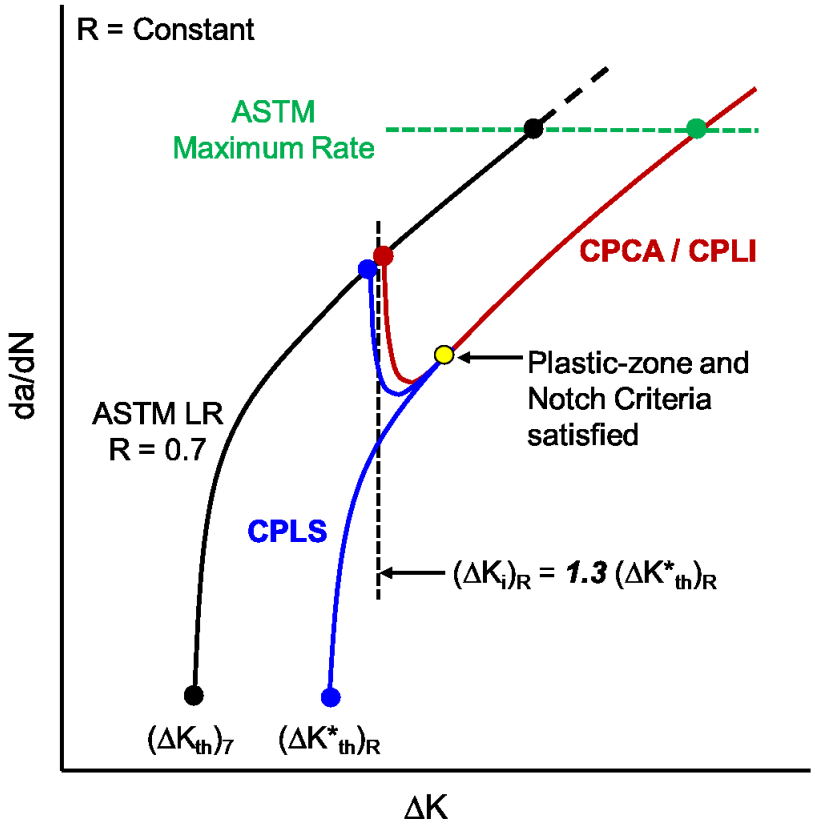

Figure 3.3 Compression pre-cracking procedures to generate near-threshold and threshold fatigue crack growth data.

CHAPTER IV

MATERIAL AND SPECIMEN CONFIGURATION

4.1 Material

The titanium alloy (Ti-6Al-4V) in solution treated and overaged (STOA) condition, produced per AMS 4928, was used for the threshold fatigue crack growth behavior study. The material yield stress (σ_{ys}) is 931 MPa (135 ksi), the ultimate tensile strength (σ_u) is 979 MPa (142 ksi), and the modulus of elasticity (E) is 116 GPa (16,800 ksi) [32].

While the material was processed in a way to minimize residual stresses, a slitting method [32, 42] was used to ensure residual stresses do not influence the crack growth measurements during the test. Using the wire electrical-discharge machining, crack length extensions were made, and residual stress-intensity factors were obtained for two standard C(T) specimens (W = 51 mm). Measured residual stress-intensity factors were less than 0.25 MPa-$\sqrt{m}$ [32] from a crack length to width ratio, a/W = 0.3 (i.e., at notch tip) to a very deep crack with a/W = 0.875 for both C(T) specimens.

4.2 Specimen configuration

The specimens were standard plan-form compact C(T) specimens as defined in the ASTM Standard E647 [22]. The specimens were machined to two different

widths, W, of 51 mm (2 in) and 76 mm (3 in) with nominal thickness, B = 6.35 mm (0.25 in). To minimize the influence of out-of-plane bending during cyclic tensile loading on the crack front shapes, the tensile load bearing part of the two pin-holes were manually beveled using a circular file.

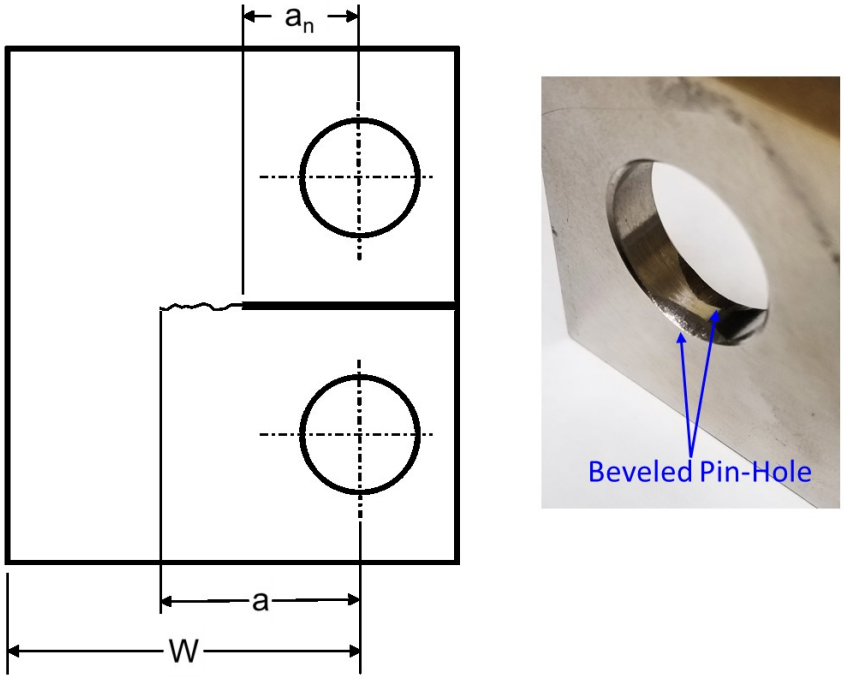

Figure 4.1 A schematic of the compact C(T) specimen.

A crack-starter U-notch was achieved by using wire electrical-discharge machining on eight of nine specimens with crack-starter-notch-to-width ratio, a_n/W, of 0.3 or 0.45. These specimens had a notch height, h = 0.5 mm (0.02 in) and a notch-tip-root radius of 0.25 mm. (0.01 in.). One C(T) specimen with W = 51 mm (2 in) had a machined starter V-notch, with crack-starter-notch to width ratio, a_n/W = 0.3, notch-tip-root radius of 0.1 mm (0.004 in) and included angle of 60°.

CHAPTER V

TEST PROCEDURES AND RESULTS

Tests for this study were performed using an Instron 8872 25 kN (5.6 kip) servo-hydraulic test machine under laboratory air conditions. Test control and data acquisition was provided by using the Fatigue Technology Associates (FTA) crack-monitoring system [43]. During each test, the crack length was continuously monitored by using the back-face compliance procedure with a back-face strain gage (BFS), as outlined in ASTM Standard E647 [22]. Crack length was periodically verified by visual measurements using an optical travel microscope. Each test was paused, and the compliance crack length was recalibrated for any large deviation in the visually observed crack length.

BFS and crack-monitoring software used back-face compliance to monitor and record the crack length and load versus strain (or displacement) data. Further, the software determined crack-opening load (P_o/P_{max}) at various compliance offset values using Elber's reduced-strain approach [44]. The ASTM Standard E647 [22] Appendix X2 recommends using 2% compliance offset (OP2) change to determine P_o/P_{max} from the load-reduced-strain (or displacement) records. However, in the current study, the OP1 (1% compliance offset) and OP2 (2 % compliance offset)

values obtained from the FTA crack-monitoring system were used to extrapolate the OP0 (0% compliance offset) value, which is closer to Elber's crack-opening load [38].

5.1 Tests using the compression pre-cracking procedure

The compression pre-cracking (CP) test procedure was used to generate fatigue crack growth rate data in the threshold and near-threshold regimes, without appreciable load-history effects at a load ratio, R = 0.1. The compact C(T) specimens were loaded using standard round pins and compression pre-cracked at high load ratios (R ≈ 20 to 50) with compressive stress-intensity factor, |Kcp|/E, of 0.00013-0.00024 $\sqrt{m}$ (0.0008-0.0015 $\sqrt{in}$) for approximately 40,000 cycles at nominal cyclic frequency of 8 or 10 Hz. While the fatigue pre-crack was not visible using the optical microscope, the FTA system detected initiation of a small crack at the notch based on the back-face compliance. The available FTA system did not possess the capability to record the crack-length under the compression-compression loading.

The specimens were then subjected to a constant-amplitude tensile loading, to overcome the residual stresses at the crack front and the notch effects. The cracks were grown to a definite length to meet the crack-extension criteria. Further, data from threshold to near fracture was obtained using either the CPLR and CPCA or CPLI test procedures, at the desired constant load ratio, and at a nominal cyclic frequency of 18 Hz. Tests were conducted on 51 mm (2 in) and 76 mm (3in) wide compact specimens.

Fatigue crack growth tests were conducted at several normalized K-gradient (C) values. All CPLS tests to obtain ΔK_{th} were followed by CPLI tests, to 'trace' back up

the crack growth rate curve. Constant K_{max} tests were also conducted at two K_{max} values of 20 MPa-√m and 11 MPa-√m. Table 5.1 summarizes the key test parameters during the CP procedures. Figure 5.1 illustrates all the near-threshold and threshold fatigue crack growth rate test data for specimens subjected to CP test procedures.

Table 5.1 Summary of key test parameters during the compression pre-cracking procedures.

Specimen ID#	Specimen Width, W (mm)	Compression Pre-Cracking	Constant Amplitude Crack-Extension	Test# 1	Test# 2
T8	51	P_{mean} = -725 lbs P_{alt} = 675 lbs N = 80002 cycles	$P_{max,i}$ = 365 lbs R = 0.7 N = 1029008 cycles Δa = 0.4172 mm	CPLI C = +0.12 mm^{-1} R = 0.7 ΔK_i = 2.97 MPa-√m P_{max} = 365 lbs	
TiD1	51	P_{mean} = -575 lbs P_{alt} = 525 lbs N = 40005 cycles	$P_{max,i}$ = 1100 lbs R = 0.6 N = 126995 cycles Δa = 0.7493 mm	Constant Kmax K_{max} = 20 MPa-√m C = -0.12 mm^{-1} ΔK_i = 8 MPa-√m	
T2	76	P_{mean} = -930lbs P_{alt} = 880lbs N = 40009 cycles	$P_{max,i}$ = 358 lbs R = 0.1	CPLI C = +0.08 and 0.16 mm^{-1} R = 0.1 ΔK_i = 4.58 MPa-√m P_{max} = 358 lbs	Constant K_{max} Kmax = 11 MPa-√m C = -0.08 and -0.16 mm^{-1} ΔK_i = 5.48 MPa-√m
T3	51	P_{mean} = -1225 lbs P_{alt} = 1175 lbs N = 40006 cycles	$P_{max,i}$ = 358 lbs R = 0.1 N = 1799481 cycles Δa = 1.2021 mm	CPLS C = -0.32 mm^{-1} R = 0.1 ΔK_i = 4.76 Pmax = 385 lbs	CPLI C = +0.32 mm^{-1} R = 0.1 ΔK_i = 3.89 P_{max} = 286.10 lbs

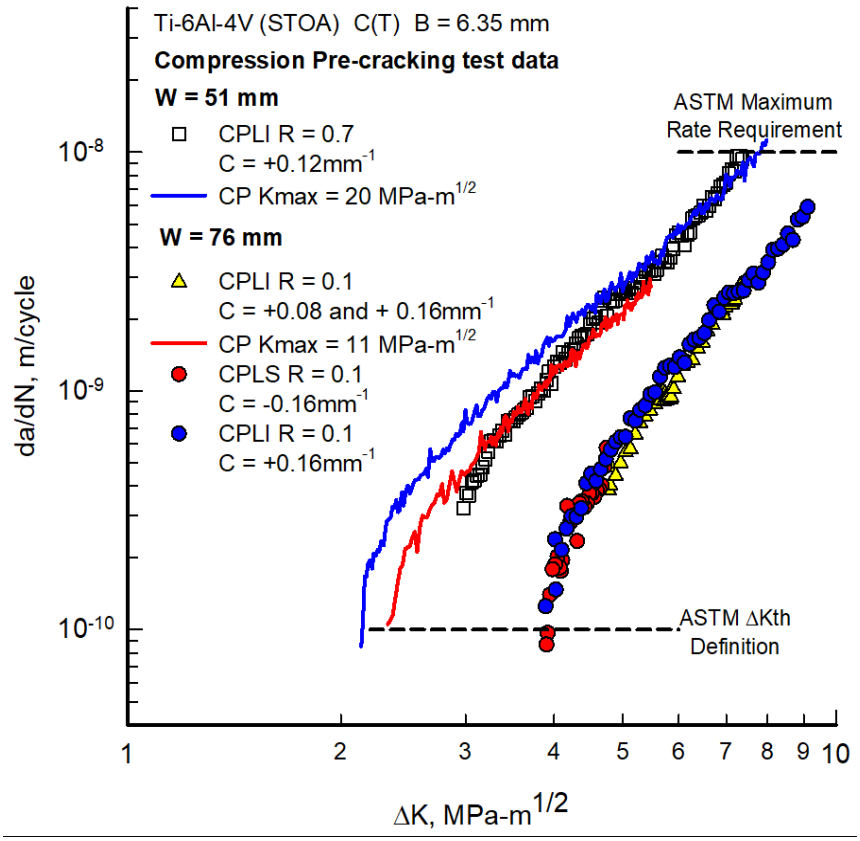

Figure 5.1 Near-threshold and threshold fatigue crack growth rate test data for compression pre-cracking test procedures.

In Figure 5.1, the dashed line at 10^{-8} m/cycle indicates the ASTM maximum rate requirement for fatigue pre-cracking followed by initiation of the threshold fatigue crack growth tests. The other dashed line at 10^{-10} m/cycle represents the ASTM Standard E647 definition for fatigue crack growth rate threshold and is included to help the reader observe and ascertain the ΔK_{th} values.

5.2 Tests using the proposed load-shedding procedure

The C(T) specimens were fatigue pre-cracked under constant-amplitude tensile loading at low stress ratio, R = 0.1. The initial starting load levels were carefully selected to ensure that the immediate crack growth rates less than 10^{-8} m/cycle (4 x 10^{-7} in/cycle). The crack was grown to a specified distance (typically 1-2 mm or 0.04-0.08 in) away from the machined crack-started notch, to overcome the possible notch effects.

Tests was then conducted to obtain near-threshold and threshold fatigue crack growth rate test data at R = 0.1, and at a range of load shed rates as the crack grew. Tests comprising normalized K gradient (C) values of -0.08 mm^{-1} (-2in^{-1}), -0.16 mm^{-1} (-4 in^{-1}), -0.32 mm^{-1} (-8 in^{-1}) and -0.95 mm^{-1} (-24 in^{-1}) were performed. All the load-shedding (LS) tests were followed by load-increasing (LI) tests at the same load ratio, intended to follow back up the crack growth rate curve. Specimens with widths, W, of 51 mm (2 in) and 76mm (3 in) were tested, at a nominal cyclic frequency of 18 Hz.

Table 5.2 summarizes the key test parameters during all the LS procedures. Figures 5.2 and 5.3 show all the near-threshold and threshold fatigue crack growth rate test data for 51 and 76mm wide specimens respectively, subjected to the proposed load-shedding test procedures.

Table 5.2 Summary of key test parameters during the load shedding procedures on 51 and 76 mm wide specimens.

Specimen ID#	Specimen Width, W (mm)	Constant Amplitude Fatigue Pre-Cracking	Test# 1	Test# 2
Ti5	51	$P_{max,i}$= 360 lbs. R = 0.1 N = 290921 cycles Δa = 1.0906 mm	LS C = -0.95 mm^{-1} R = 0.1 ΔK_i = 8.67 MPa-√m $P_{max,i}$ = 360 lbs.	LI C = +0.95 mm^{-1} R = 0.1 ΔK_i = 4.18 MPa-√m $P_{max,i}$ = 166 lbs.
Ti6	51	$P_{max,i}$ = 360 lbs. R = 0.1 N = 260980 cycles Δa = 1.2721 mm	LS C = -0.32 mm^{-1} R = 0.1 ΔK_i = 9.02 MPa-√m $P_{max,i}$ = 360 lbs.	LI C = +0.32 mm^{-1} R = 0.1 ΔK_i = 3.98 MPa-√m $P_{max,i}$ = 136 lbs.
Ti7	51	$P_{max,i}$ = 360 lbs. R = 0.1 N = 281646 cycles Δa = 1.1442 mm	LS C = -0.08 mm^{-1} R = 0.1 ΔK_i = 9.07 MPa-√m $P_{max,i}$ = 360 lbs.	LI C = +0.16 mm^{-1} R = 0.1 ΔK_i = 4.72 MPa-√m $P_{max,i}$ = 93.90 lbs.
T1	76	$P_{max,i}$ = 700 lbs. R = 0.1 N = 224242 cycles Δa = 1.1404 mm	LS C = -0.32 mm^{-1} R = 0.1 ΔK_i = 9.35 MPa-√m $P_{max,i}$ = 700 lbs.	LI C = +0.32 mm^{-1} R = 0.1 ΔK_i = 4.08 MPa-√m $P_{max,i}$ = 279.10 lbs.
T4 (Part A)	76	$P_{max,i}$ = 690 lbs. R = 0.1 N = 262848 cycles Δa = 1.2739 mm	LS C = -0.95 mm^{-1} R = 0.1 ΔK_i = 9.35 MPa-√m $P_{max,i}$ = 690 lbs.	LI C = +0.32 mm^{-1} R = 0.1 ΔK_i = 5.32 MPa-√m $P_{max,i}$ = 381.10lbs.
T4 (Part B)			LS C = -0.32 mm^{-1} R = 0.1 ΔK_i = 8.90 MPa-√m $P_{max,i}$ = 603.90 lbs.	LI C = +0.32 mm^{-1} R = 0.1 ΔK_i = 4.77 MPa-√m $P_{max,i}$ = 301.10 lbs.

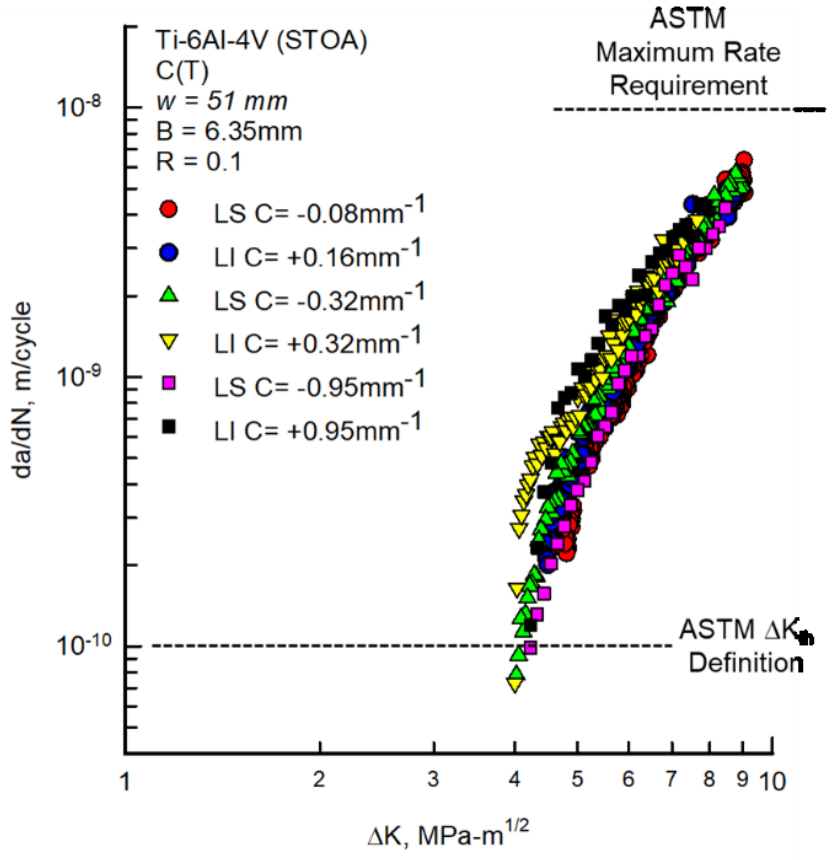

Figure 5.2 Near-threshold and threshold fatigue crack growth rate test data for specimen width, W = 51 mm, using the proposed load-shedding test procedure.

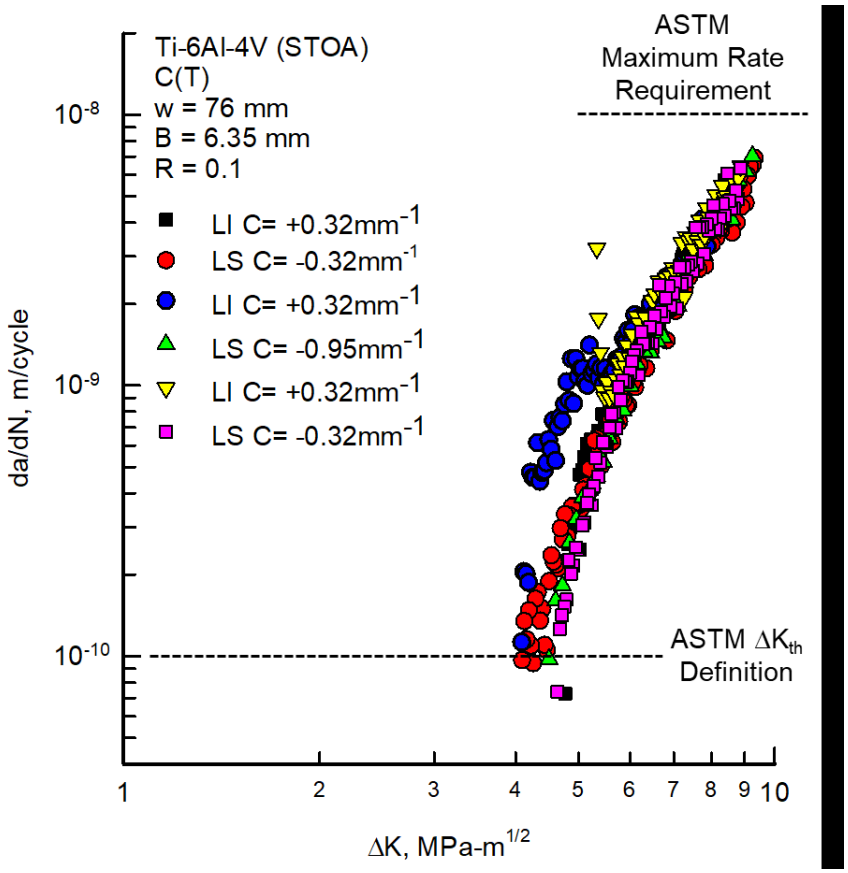

Figure 5.3 Near-threshold and threshold fatigue crack growth rate test data for specimen width, W = 76 mm, using the proposed load-shedding test procedure.

CHAPTER VI

DISCUSSION OF TEST RESULTS

6.1 Previous tests on Ti-6Al-4V (STOA) by Newman et al. [27, 32]

Newman et al. [27, 32] performed near-threshold and threshold fatigue crack growth tests on a Ti-6Al-4V (STOA) alloy, with specimen widths W = 25, 51, and 76 mm, at various stress ratios (R = 0.1, 0.4, and 0.7) using the current ASTM Standard E647 LR [22] and the CPCA test procedures. The test results from these procedures are discussed in this section.

LR test procedure fatigue crack growth data [32] for 25, 51, and 76 mm wide specimens, at various load ratios (i.e., R = 0.1, 0.4, and 0.7) is presented in Figure 6.1. At a same ΔK value, faster fatigue crack growth rates are observed at high Rs. Further, the ΔK_{th} value (at 10^{-10} m/cycle) varies as a function of R. The LR test data is expected to exhibit such a load ratio effect, due to build-up of various crack-closure mechanisms as ΔK-decreases (i.e., loads are shed). R = 0.1 test data shows a "fanning out" of ΔK values at lower crack growth rates as a function of specimen width, i.e., a large scatter of ΔK values is observed between 51 and 76 mm wide specimens below $1E^{-9}$ m/cycle. Further, for a given ΔK value, the wider 76 mm specimen produces lower crack growth rates than the narrower 51 mm specimen. Such specimen width effects reveal an unexpected trend similar to that observed when the LR test

procedure was used on Inconel-718 [45]. For R = 0.4 test data, the accelerated crack growth in narrower specimens was not as pronounced as for R = 0.1. No LR R = 0.4 test attained threshold fatigue crack growth rates of 10^{-10} m/cycle. For a given ΔK, below $2E^{-9}$ m/cycle, the 76 mm wide specimen produced slower fatigue crack growth rates than the 25 or 51 mm wide specimens. The high R = 0.7 crack growth rate data in the Figure 6.1 is a mix of fatigue crack growth rates generated from the LR and CPCA test procedures. These LR and CPCA test data agree well within the experimental scatter.

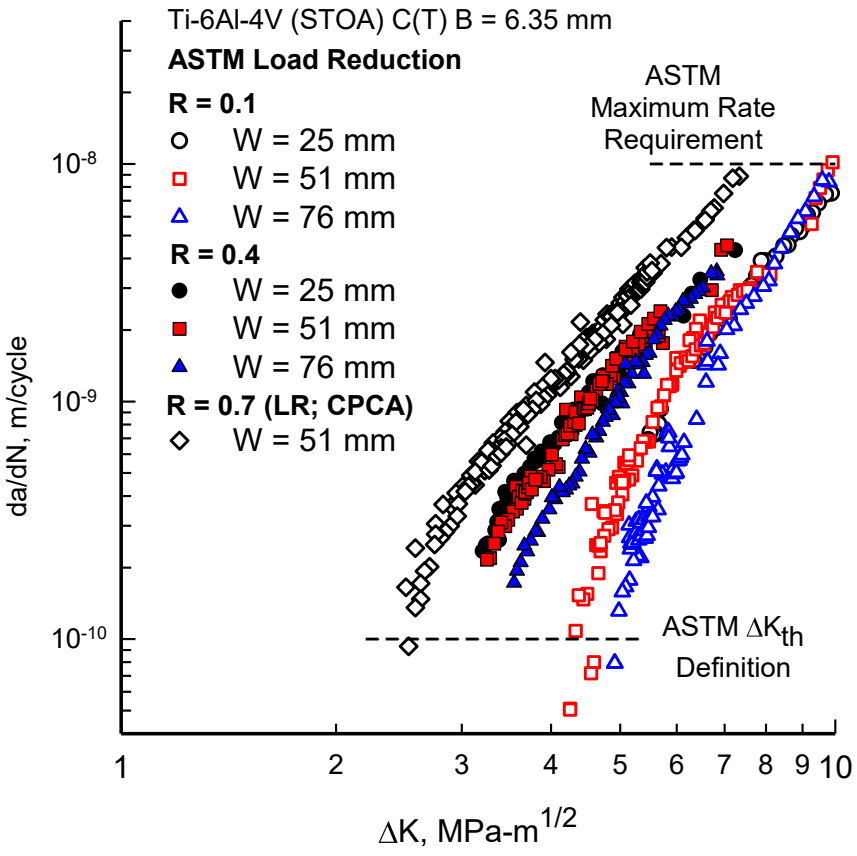

Figure 6.1 Threshold fatigue crack growth data by Newman et al. [32] for Ti-6Al-4V (STOA) using the load-reduction (LR) test procedure.

Fatigue crack growth test data at various load ratios (i.e., R = 0.1, 0.4, and 0.7), using the CPCA [32] test procedure on 25, 51, and 76 mm wide specimens is presented in Figure 6.2. In contrast to the LR R = 0.1 tests (Figure 6.1), no specimen width effect can be observed in the CPCA R = 0.1 test data. The CPCA test fatigue crack growth data for the three specimen widths (i.e., W = 25, 51, and 76 mm) plot directly on top of each other for the same range of crack growth rates. Also, the CPCA R = 0.1 test procedures produce lower ΔK_{th} values (at 10^{-10} m/cycle) in comparison to the LR R = 0.1 tests (Figure 6.1).

R = 0.4 CPCA [32] tests (Figure 6.2) show a slight influence of the specimen width effect above $3E^{-10}$ m/cycle, where the 76 mm wide specimen produced slower crack growth rates than the 25 or 51 mm wide specimen. However, the specimen width effect on the CPCA R = 0.4 tests are not as marked as the effect observed in the LR R = 0.4 tests (Figure 6.1). Further, crack growth rates for the 76 mm wide specimen show a good agreement with the narrower 25 and 51 mm wide specimens near the threshold regime (i.e., at about 10^{-10} m/cycle). For R = 0.7, the LR test results were similar to the CPCA tests, as was observed during testing of other materials [24, 27- 29].

As a result of these noticeable differences between the LR and CPCA test procedures [32] (in Figures 6.1 and 6.2 respectively) on R = 0.1 and 0.4 test data, Newman et al. [27, 32] concluded that the CPCA test procedures were an improvement over the LR test procedures. The CPCA test procedure offered a more accurate representation of the threshold fatigue crack growth rates and the ΔK_{th} value

in comparison to the LR test procedure. Further, at the same R, the CPCA test results were independent of the specimen widths, while the LR tests demonstrated a variance in results between different specimen widths.

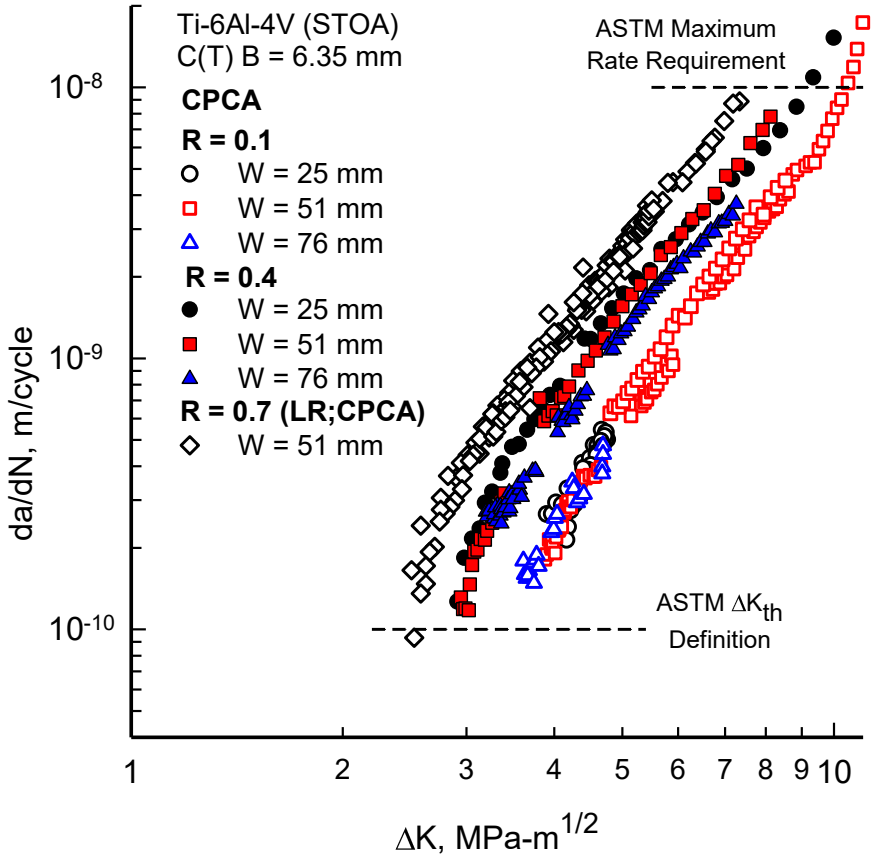

Figure 6.2 Threshold fatigue crack growth data by Newman et al. [32] for Ti-6Al-4V (STOA) using the compression pre-cracking constant amplitude (CPCA) test procedure.

The FASTRAN life-prediction code [46] was used to correlate the ΔK-da/dN data between the various load ratios. In these analyses, the LR-CPCA test data for R = 0.7 was assumed to be unaffected by the crack-closure effects, and thus $\Delta K = \Delta K_{eff}$. A solid ΔK_{eff}-da/dN curve was fitted to the R = 0.7 test data (Figure 6.3). Based on the

fitted ΔK_{eff}-da/dN curve, FASTRAN [46] crack closure predictions were made for R = 0.1 and 0.4 data (presented by solid curves in Figure 6.3), with a tensile constraint factor α = 1.9. The CPCA test data [32] matches the FASTRAN predictions very well for the low stress ratios. These predicted FASTRAN (α = 1.9) solid curves in Figure 6.3 will be used as a reference point in further discussion and analyses of the test data from the current study for this thesis.

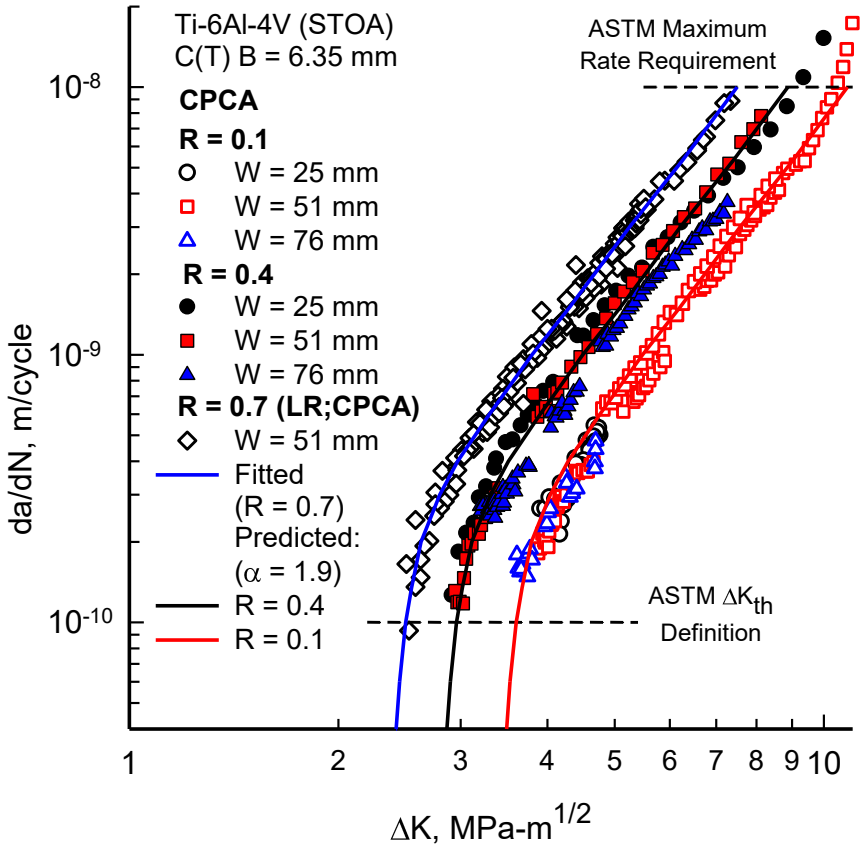

Figure 6.3 Compression pre-cracking constant-amplitude (CPCA) threshold fatigue crack growth data by Newman et al. [32] plotted with the predicted FASTRAN [46] curves.

One of the objectives of this research is to compare the prior LR and CPCA test data [32], with the LS and CP test data (discussed in Chapter 5) from this current study. In the following sections, a comparison between the LR, CPCA, LS and CP test procedures is presented.

6.2 Comparison of the test data for the load-reduction [32] and the load-shedding test procedures

A comparison of the fatigue crack growth rates generated using LR [32] and LS test procedures for the 51 wide mm specimens, at various load-shed rates (i.e., C = -0.08, -0.32, and -0.95 mm^{-1}), for R = 0.1 are presented in Figure 6.4. All the LS tests were initiated at similar ΔK-da/dN values, while the one LR test was initiated at a higher ΔK-da/dN value. Above 10^{-9} m/cycle, the LR, LS and the FASTRAN [46] R = 0.1 data are in a very good agreement. However, below 10^{-9} m/cycle, the LR and LS test data corresponded to higher ΔK values in comparison to the predicted FASTRAN R = 0.1 curve. Such LR and LS test behavior are indicative of the influence of various crack-closure mechanisms, due to generally decreasing ΔK values and prior the prior load-history effects, as the crack growth rates approach thresholds (at 10^{-10} m/cycle). A large scatter in the ΔK values is observed around 10^{-10} m/cycle as a function of C; they do not show a particular trend. Also, at 10^{-10} m/cycle, the LR and LS test procedures produce higher ΔK_{th} values, compared to that predicted by FASTRAN for R = 0.1. Further, as is expected, higher Cs (-0.32 or -0.95 mm^{-1})

produced faster fatigue crack growth rates for same ΔK values, than lower C = -0.08 mm^{-1}.

A fatigue crack growth rate data comparison from the R = 0.1 LR [32] and LS test procedures for the 76 mm wide specimens at various load-shed rates (i.e., C = -0.08, -0.32, and -0.95 mm^{-1}) are presented in Figure 6.5. The LR and LS test data for the 76 mm wide specimens show similar trends to that for the 51 mm wide specimens (Figure 6.4). All the LR and LS tests on the 76 mm wide specimens were initiated at similar ΔK-da/dN values. Above $2E^{-9}$ m/cycle, the LR, LS and the FASTRAN [46] R = 0.1 data are all in very good agreement. However, below $2E^{-9}$ m/cycle, the LR and LS test data begin to deviate towards higher ΔK values in comparison to the predicted FASTRAN curve, due to generally decreasing ΔK values and prior load-history effects leading to a build-up of various crack-closure mechanisms, as the crack growth rates approach threshold.

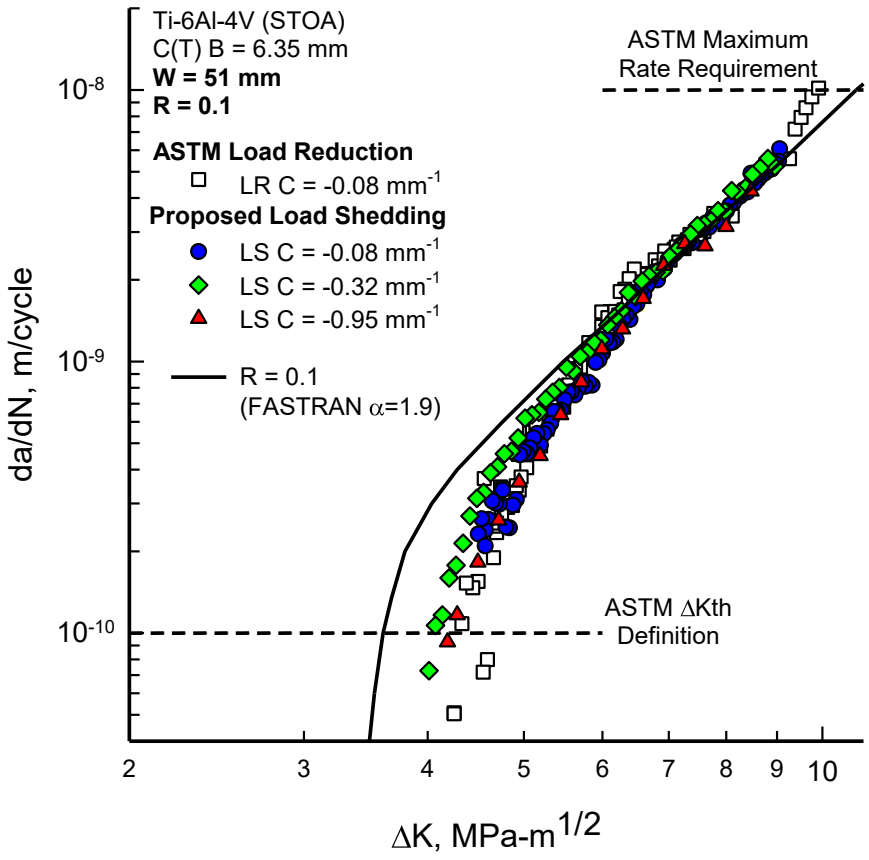

Figure 6.4 Comparison of fatigue crack growth rate data from the load-reduction (LR) [32] and the load-shedding (LS) test procedures for R = 0.1 and W = 51 mm.

Further, a large scatter in the ΔK values is observed at around 10^{-10} m/cycle as a function of C (Figure 6.5), and higher C values (-0.32 or -0.95 mm^{-1}) produced faster fatigue crack growth rates than C = -0.08 mm^{-1}. Also, at 10^{-10} m/cycle, the R = 0.1 LR and LS test procedures produce higher ΔK_{th} values compared to that predicted by FASTRAN [46]. In comparison, the ΔK_{th} values for the 76 mm wide specimens were higher than the ΔK_{th} values for the 51 mm wide specimens (Figure 6.4). To recap, both the LR [32] and LS test procedures are influenced by

various crack-closure mechanisms and load-history effects that lead to higher thresholds than predicted by FASTRAN.

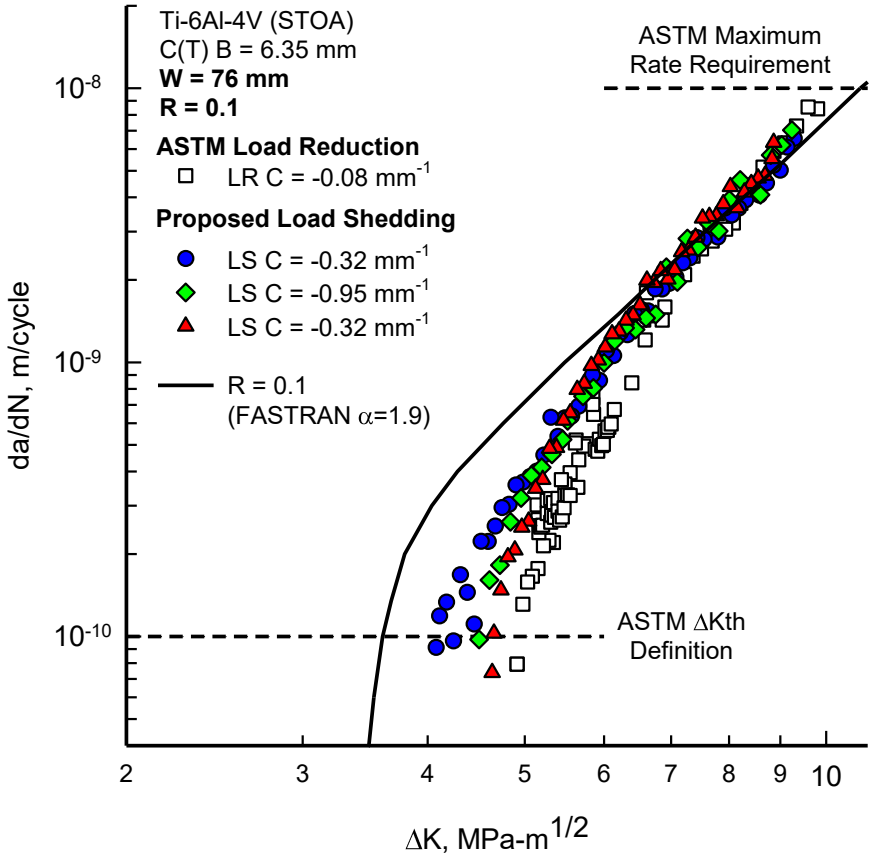

Figure 6.5 Comparison of fatigue crack growth rate data from the load-reduction (LR) [32] and the load-shedding (LS) test procedures for R = 0.1 and W = 76 mm.

6.3 Specimen width effect in the load shedding test procedures

Test data from all the R = 0.1 LR [32] and LS test procedures on 51 and 76 mm wide specimens are presented in Figure 6.6. The test results show a large variance in ΔK values below $2E^{-9}$ m/cycle. All the LS tests from the current study were initiated

at similar ΔK-da/dN values, and the two LR tests were initiated at higher ΔK-da/dN values slightly above the ASTM maximum rate requirement (dashed line at 10^{-8} m/cycle). In the near-threshold region below $2E^{-9}$ m/cycle, for the same ΔK and C values, 76 mm specimens produce slower rates than the 51 mm wide specimens. Further, at threshold (ΔK_{th} at 10^{-10} m/cycle), 76 mm wide specimens also produce noticeably higher ΔK_{th} values than the 51 mm wide specimens. As discussed in Section 6.1 (Figure 6.1), Newman et al. [32] observed similar specimen width effects, where for the same R, wider specimens (i.e., W = 76 mm) produce higher thresholds and slower rates in comparison to the narrower specimen (i.e., W = 51 mm).

For a given R value, the LR and LS test employing decreasing ΔK values produce different thresholds depending on the specimen width; this result calls into question the utility of these two methods. Further, the specimen width dependence on the generated fatigue crack growth rates is a clear violation of certain fracture mechanics concepts, where crack growth rate behavior can be correlated with the alternating stress-intensity factor range for a given load ratio.

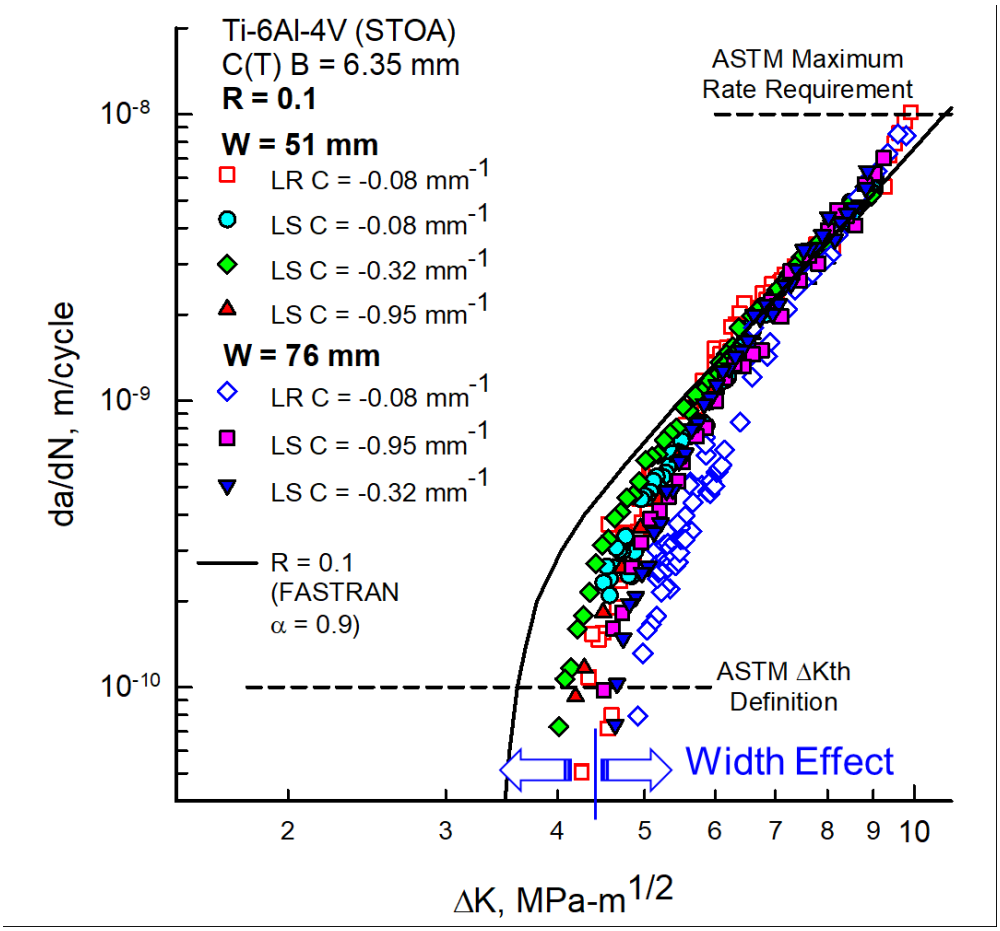

Figure 6.6 Specimen width effect in the load reduction (LR) and load shedding (LS) test procedures.

6.4 Comparison of the test data for the load-reduction [32] and the compression pre-cracking test procedures

Fatigue crack growth data for the 76 mm wide specimens from the LR test procedures by Newman et al. [32] and the CP test procedures from the current study are presented in Figure 6.7. As discussed in Section 6.3, for a given R, the LR test methods produce fatigue crack growth rates and thresholds that depend on the specimen width. Hence, for a consistent analyses between the LR and CP test datasets,

specimen widths of 25 and 51 mm are excluded in this comparison. A large disparity in the ΔK values for the same examined crack growth rates is observed between the LR and CP test results below 10^{-9} m/cycle. The LR and CP test data agree fairly well with the FASTRAN [46] R = 0.1 prediction above $2E^{-9}$ and $4E^{-10}$ m/cycle, respectively. Below these rates, test data from both LR and CP test methods produce higher ΔK values than the FASTRAN R = 0.1 curve for the same crack growth rate.

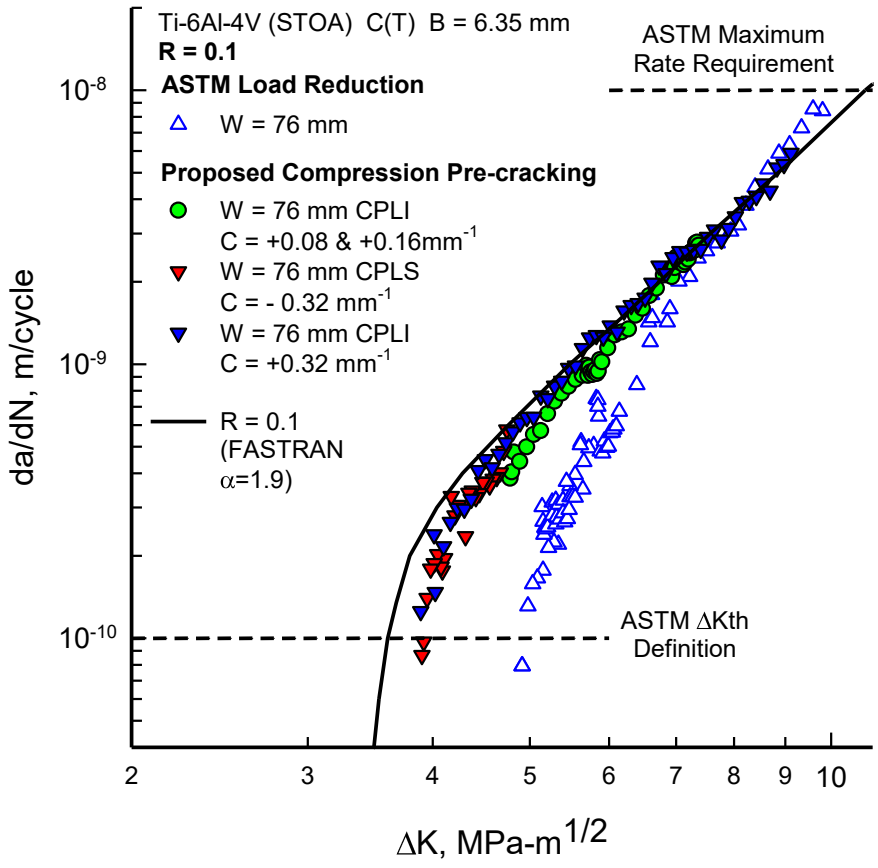

Figure 6.7 Comparison of fatigue crack growth data from the load-reduction (LR) [32] and the compression pre-cracking (CP) test procedures for R = 0.1 and W = 76 mm.

An expanded view of the LR and CP test results for rates below 10^{-9} m/cycle, are presented in Figure 6.8 to help in better visualization of the fatigue crack growth behavior in the threshold regime. The LR test procedure produces a ΔK_{th} value of 4.95 MPa-√m, that is 40 % higher than the estimated $(\Delta^* K_{th})_{R=0.1}$ value. In contrast, the ΔK_{th} from the CPLS test is 3.91 MPa-√m (i.e., 10 % higher than the estimate). No test procedure provides a definitive measure of the ΔK_{th} value and the threshold fatigue crack growth rates. However, the CPLS test procedure is a *significant* improvement over the LR test procedure and offers a more accurate alternative for determination of the ΔK_{th} value and the threshold fatigue crack growth rates.

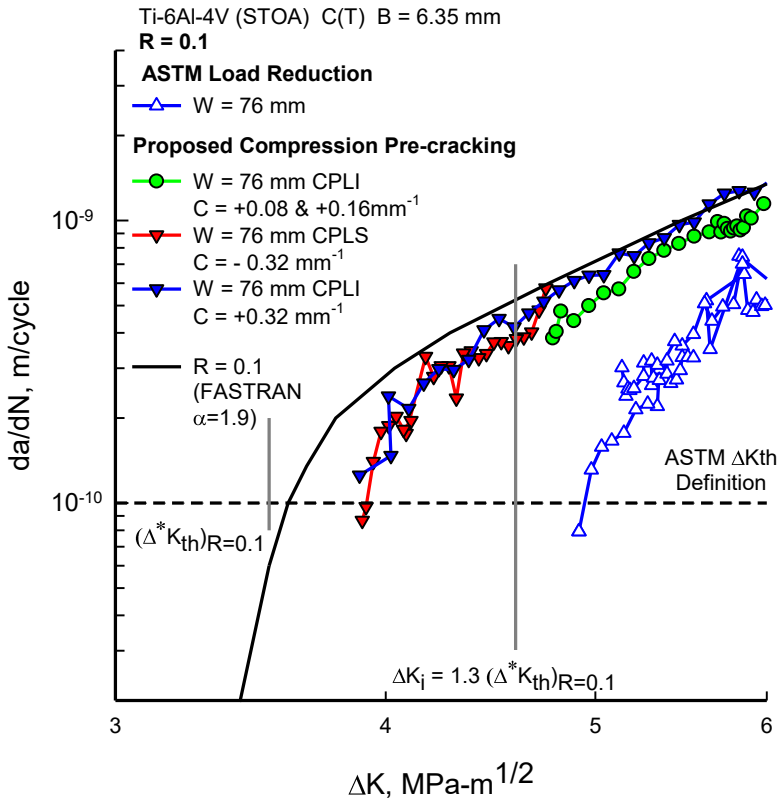

Figure 6.8 An expanded view of the threshold fatigue crack growth data from the load-reduction (LR) [32] and the proposed compression pre-cracking (CP) test procedures for R = 0.1 and W = 76 mm.

6.5 Comparison of the test results for the compression pre-cracking constant amplitude [32] and the proposed load-shedding test procedures

R = 0.1 fatigue crack growth tests results on a 51 mm wide specimen using the CPCA [32] procedure and the LS procedure is presented in Figure 6.9. The CPCA test produced fatigue crack growth rates independent of the specimen width. The CPCA test data for three specimen widths (i.e., 25, 51, and 76 mm) plotted directly on top of each other for the same examined crack growth rates. Also, the CPCA test results show a good agreement with the predicted FASTRAN [46] R = 0.1 curve. The LS test data for the 51 mm specimens also agrees well the FASTRAN R = 0.1 curve above 10^{-9} m/cycle. Below 10^{-9} m/cycle, the LS test produces higher ΔK values and slower rates than the CPCA tests. In the threshold region (i.e., at around 10^{-10} m/cycle), the LS tests are affected by prior load-history and a build-up of various crack-closure mechanisms resulting in to slower crack growth rates. As a result, the LS test produced significantly higher ΔK_{th} values than predicted by the FASTRAN R = 0.1 curve.

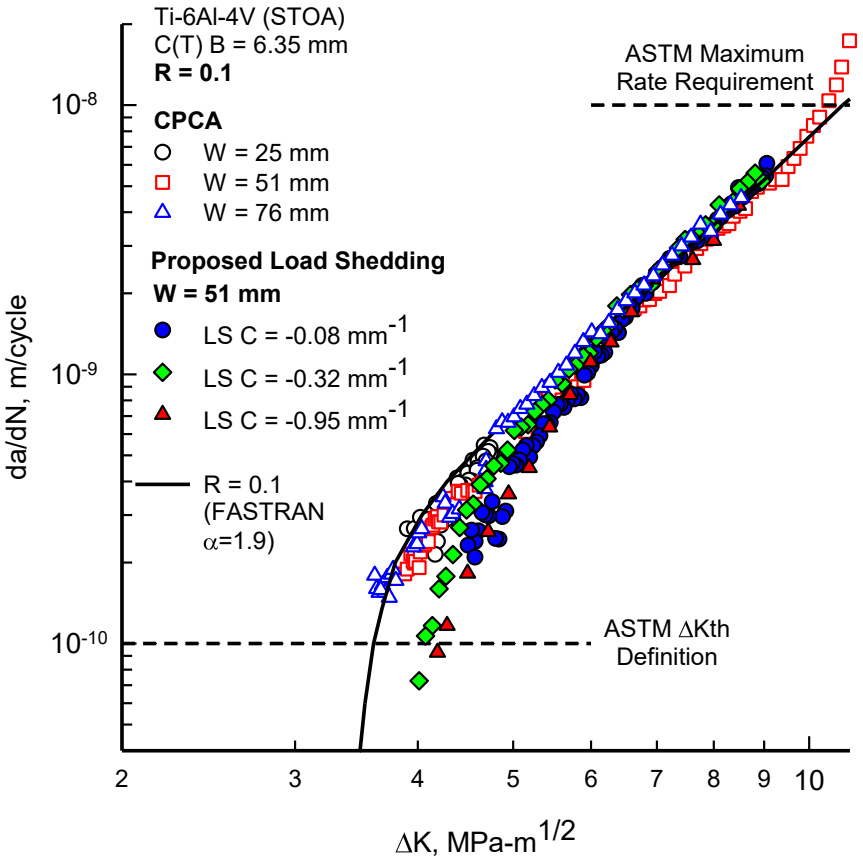

Figure 6.9 Comparison of fatigue crack growth data from the compression pre-cracking constant amplitude (CPCA) [32] and the load-shedding (LS) test procedures for R = 0.1 and W = 51 mm.

A comparison of the R = 0.1 fatigue crack growth tests results on a 76 mm wide specimen using the CPCA [32] procedure and the LS procedure is presented in Figure 6.10. The CPCA test data in Figure 6.10 is similar to that discussed previously (Figure 6.9). Furthermore, the LS test data for the 76 mm specimens (Figure 6.10) agrees well the FASTRAN [46] R = 0.1 curve above $2E^{-9}$ m/cycle. Below $2E^{-9}$ m/cycle, the LS tests produce higher ΔK values and slower rates than the CPCA tests. Similar to the observations made for Figure 6.9, the LS tests for the 76 mm wide specimen in

Figure 6.10 are affected by various crack-closure mechanisms leading to slower crack growth rates in the threshold region (i.e., around 10^{-10} m/cycle). The LS tests on 76 mm produced significantly higher ΔK_{th} values, and marginally higher than LS ΔK_{th} values for 51mm specimens in Figure 6.9, in comparison to that predicted by the FASTRAN R = 0.1 curve. In summary, the CPCA test method provided a better representation of the threshold fatigue crack growth rates, than the proposed LS test method.

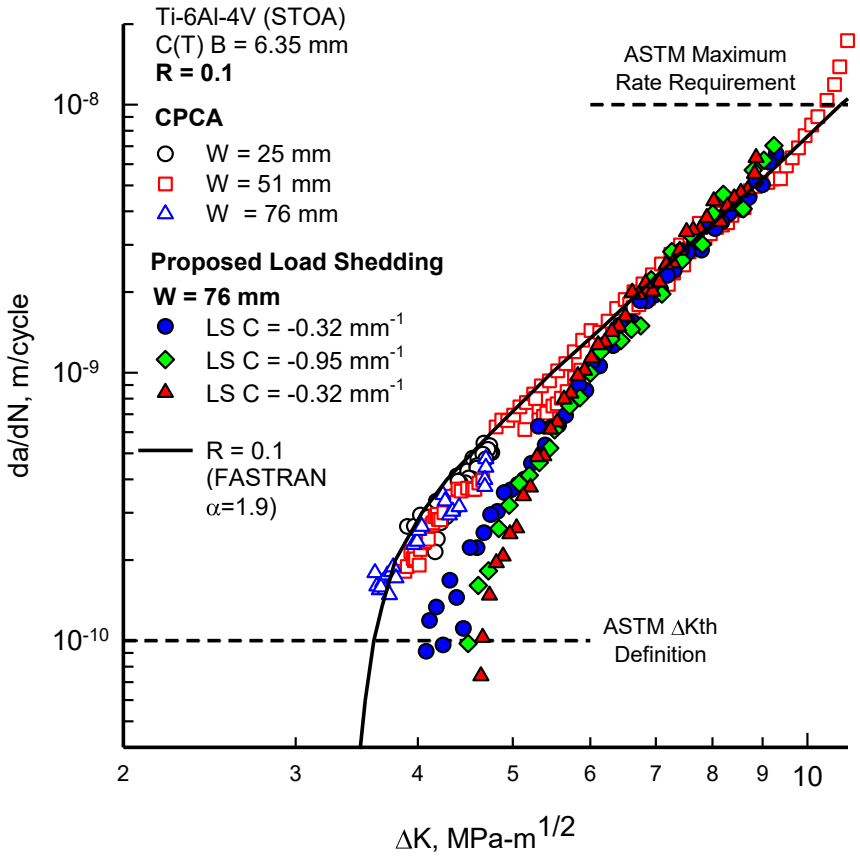

Figure 6.10 Comparison of fatigue crack growth data from the compression pre-cracking constant amplitude (CPCA) [32] and the load-shedding (LS) test procedures for R = 0.1 and W = 76 mm.

6.6 Comparison of the test data for the compression pre-cracking constant amplitude [32] and the proposed compression pre-cracking test procedures

High R = 0.7 fatigue crack growth test data for 76 mm wide specimen, using the LR-CPCA [32] and the CPLI test procedure are presented in Figure 6.11. As discussed in Section 6.1, the R = 0.7, CPCA test data agreed very well with the LR tests. A CPLI (at C = +0.32 mm^{-1}) test was performed on the 76 mm wide specimen, at R = 0.1, to study the behavior of increasing ΔK values (i.e., load-increasing) in comparison to the LR-CPCA test performed by Newman et al. [32]. The CPLI fatigue crack growth test data shows a remarkably good ΔK-da/dN agreement with the LR-CPCA test data and the fitted R = 0.7 curve, from initial crack growth rates of $3E^{-10}$ m/cycle to 10^{-8} m/cycle.

Further, the R = 0.1 fatigue crack growth rate data comparison between the CPCA [32] and the proposed CP test methods are presented in Figure 6.12. R = 0.1 CP tests (i.e., CPLS and CPLI tests at various Cs) were performed only on 76 mm wide specimens. The CPCA and CP tests show an excellent agreement of ΔK-da/dN data above $3E^{-10}$ m/cycle with no effects of variable specimen width. The predicted FASTRAN [46] R = 0.1 results under-predict the test data by about 10% at crack growth rates of ~$3E^{-10}$ m/cycle. For a better visualization of near-threshold fatigue crack growth behavior, an expanded view (fatigue crack growth rates less than 10^{-9} m/cycle) of R = 0.1 test data is provided in Figure 6.13.

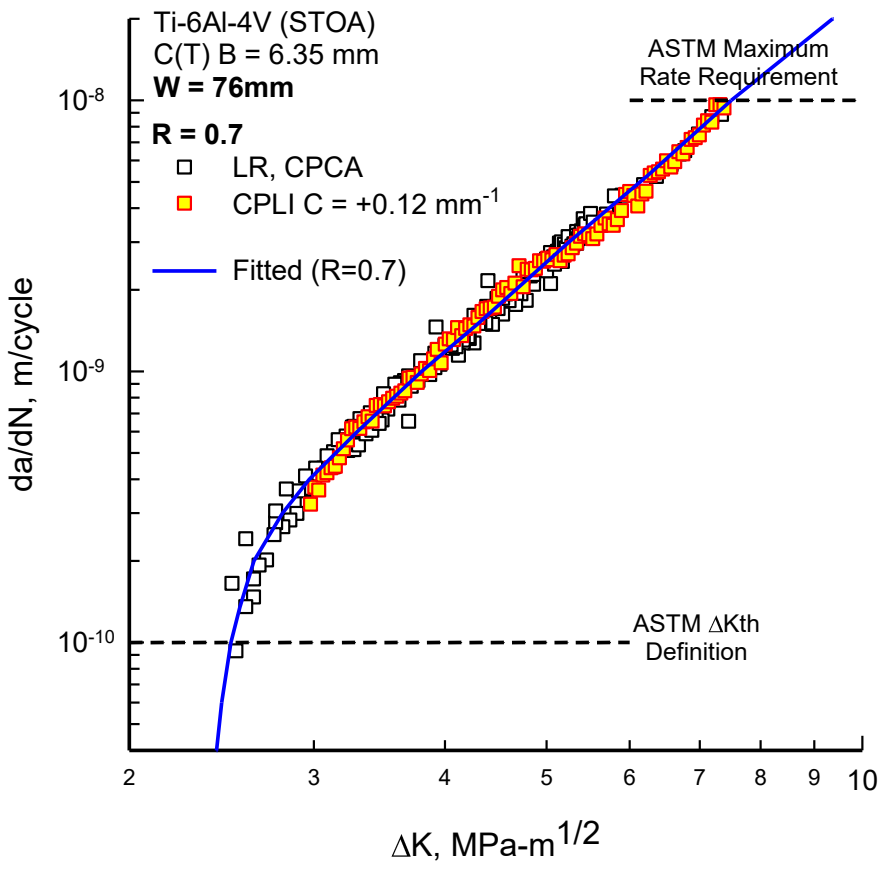

Figure 6.11 Comparison of the compression pre-cracking constant-amplitude (CPCA) [32] and the compression pre-cracking load-increasing (CPLI) test data at R = 0.7.

In Figure 6.13, the CPLS ($C = -0.32$ mm^{-1}) test begins to deviate from the CPCA [32] test data below $3E^{-10}$ m/cycle. At these fatigue crack growth rates, the CPLS test produces higher ΔK values in comparison to the CPCA test data over the range of crack growth rates. The CPLS test was initiated at a ΔK-da/dN value (i.e., at ΔK_i) which is order-of-magnitude below the established ASTM maximum test initiation rate of 10^{-8} m/cycle. Yet, the CPLS test that employs decreasing ΔK values (i.e. load-reduction) to achieve threshold fatigue crack growth rates appears to be affected by

crack-closure effects and produces a ΔK_{th} that is *10% higher* than the estimated $(\Delta^* K_{th})_{R=0.1}$. In summary, CPLS test procedure are slightly affected by the crack-closure effects at low R values. Further research is required for developing test procedure(s) capable of providing a more definitive representation of the ΔK_{th} value and closure-free fatigue crack growth rates in the threshold regime.

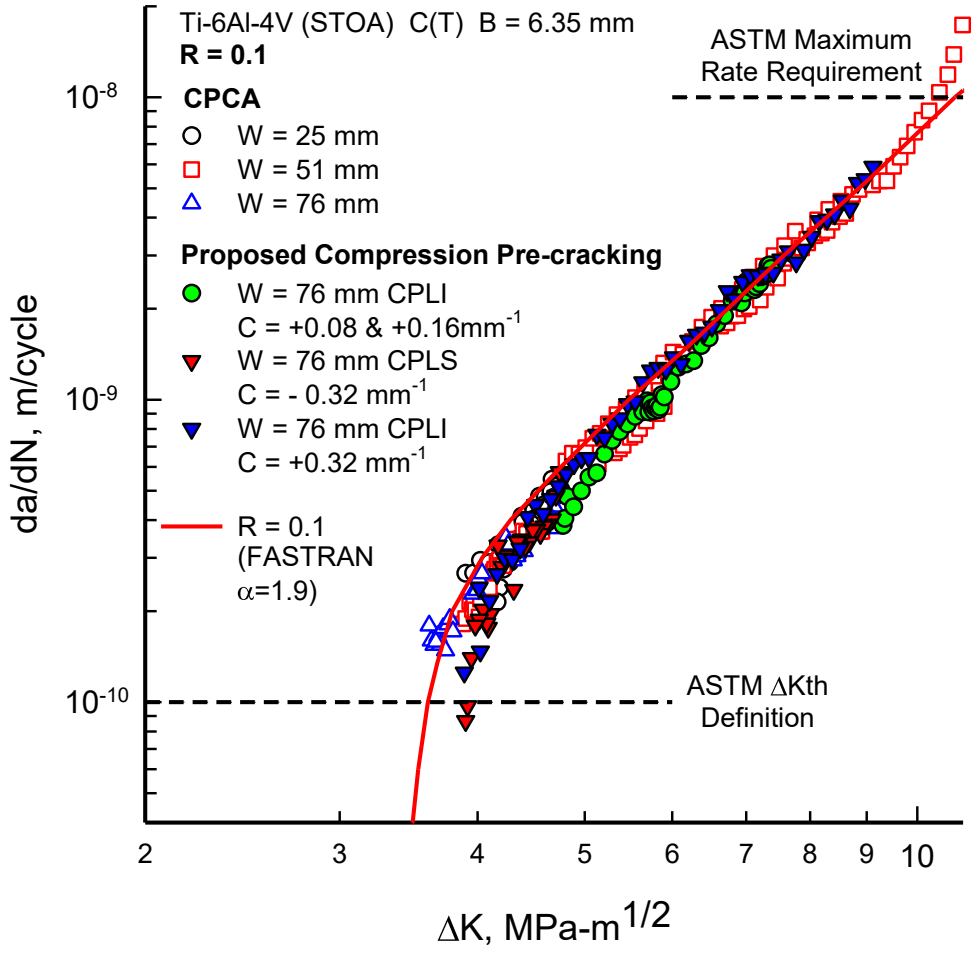

Figure 6.12 Comparison of the compression pre-cracking constant-amplitude (CPCA) [32] and the compression pre-cracking (CP) test data at R = 0.1.

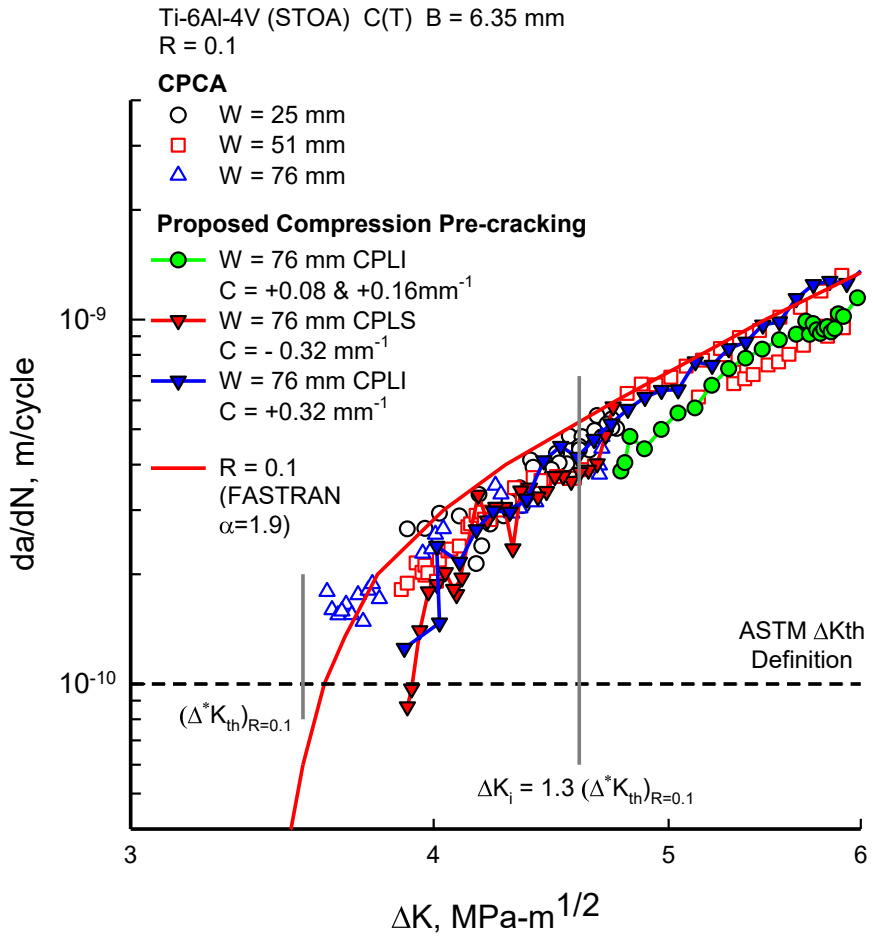

Figure 6.13 An expanded view of the threshold fatigue crack growth data from compression pre-cracking constant-amplitude (CPCA) [32] and the compression pre-cracking (CP) test data at R = 0.1.

6.7 Comparison of the current test data for the load-shedding procedures and the compression pre-cracking test procedures

A comparison of all the R = 0.1 data for proposed LS and CP test, on 51 and 76 mm wide specimens, are presented in Figure 6.14. No test procedure provides an accurate representation of the fatigue crack growth threshold $(\Delta^*K_{th})_{R=0.1}$. The CPLS test provides a better representation of ΔK_{th}, in comparison to the LS test procedures.

The LS test methods produce higher ΔK_{th} values and lower rates than the CP test procedures. A summary of ΔK_{th} values obtained for all the R = 0.1 tests, using the proposed LS and CP test procedures is presented in Table 6.1.

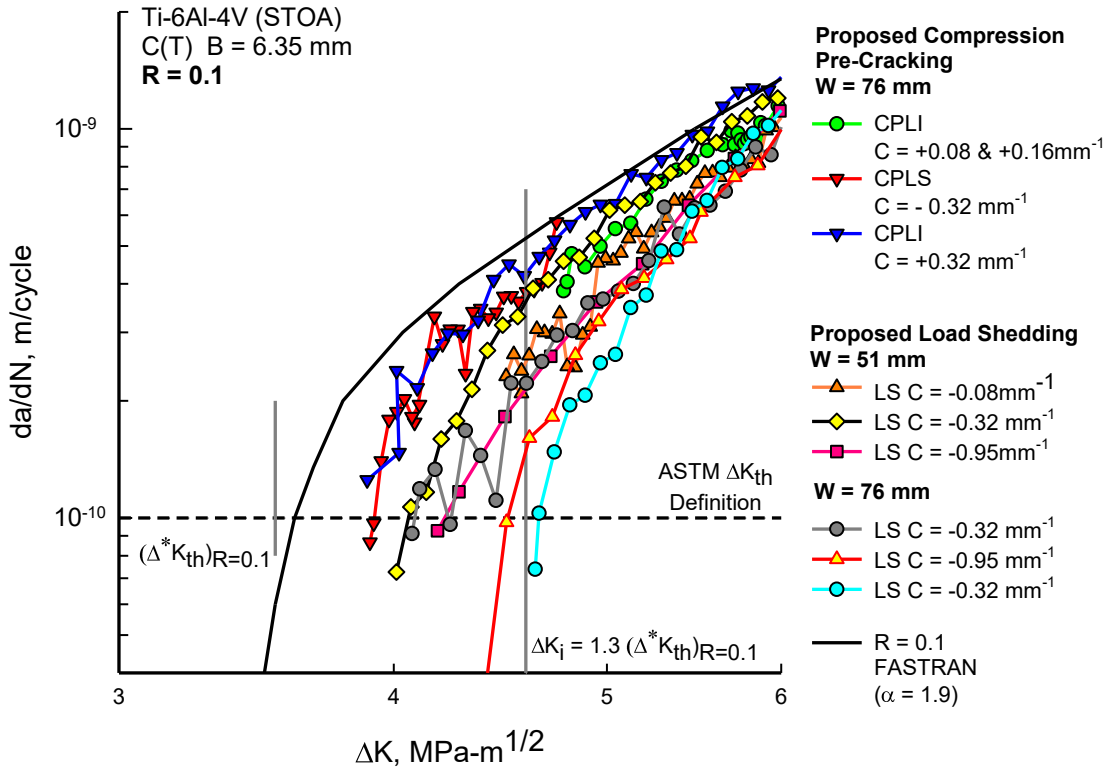

Figure 6.14 Comparison of the test data for the load-shedding (LS) and the compression pre-cracking (CP) test procedures at R = 0.1

Table 6.1 Summary of ΔK_{th} values obtained using the proposed LS and CP test procedures the R = 0.1

Test Procedure	Specimen Width	Normalized K-gradient, C	ΔK_{th} (MPa-√m) at 10^{-10} m/cycle.	Error in comparison to $(\Delta^* K_{th})_{R=0.1}$
CPLS	76 mm	-0.32 mm^{-1}	3.91	10 %

Table 6.1 Summary of ΔK_{th} values obtained using the proposed LS and CP test procedures the R = 0.1 (continued)

Test Procedure	Specimen Width	Normalized K-gradient, C	ΔK_{th} (MPa-√m) at 10^{-10} m/cycle.	Error in comparison to $(\Delta^* K_{th})_{R=0.1}$
LS	51 mm	-0.08 mm^{-1}	No ΔK_{th} at 10^{-10} m/cycle	
		-0.32 mm^{-1}	4.07	15 %
		-0.95 mm^{-1}	4.23	20 %
	76 mm	-0.32 mm^{-1}	4.09	16 %
		-0.95 mm^{-1}	4.50	27 %
		-0.32 mm^{-1}	4.67	32 %

6.8 Analyses of the crack-opening loads for the load-shedding procedures

One of the objectives of the proposed LS test procedure was to possibly produce closure-free fatigue crack growth rates in the threshold regime. However, the ΔK or K decreasing procedures (i.e., the LR and LS test procedures) are influenced by the loading-history and crack-closure due the plastically deformed material left behind in the wake of advancing crack. Crack-closure weakens the crack-tip driving force leading to higher (potentially *non-conservative*) ΔK_{th} values and slower crack growth rates in the threshold regime.

This section summarizes the observed crack-closure during LS tests on 51 mm wide specimens at various C values, based on the measured crack-opening (P_o/P_{max}) loads during the tests. OP1 (1% compliance offset) and OP2 (2% compliance offset)

values determined by the FTA [43] crack monitoring system using back-face compliance procedure and BFS were used to extrapolate a OP0 (0% compliance offset) value which is closer to Elber's crack-opening load [38]. A plot of OP0 based P_o/P_{max} on a linear scale and the fatigue crack growth rates in the threshold regime on a log scale are presented in Figure 6.15 for the LS tests at various C values (i.e., -0.08, -0.32, and -0.95 mm^{-1}) for 51 mm wide specimens. FASTRAN [46] predicted a P_o/P_{max} value of 0.3759 for $\alpha = 1.9$ and R = 0.1, is also include in the figure.

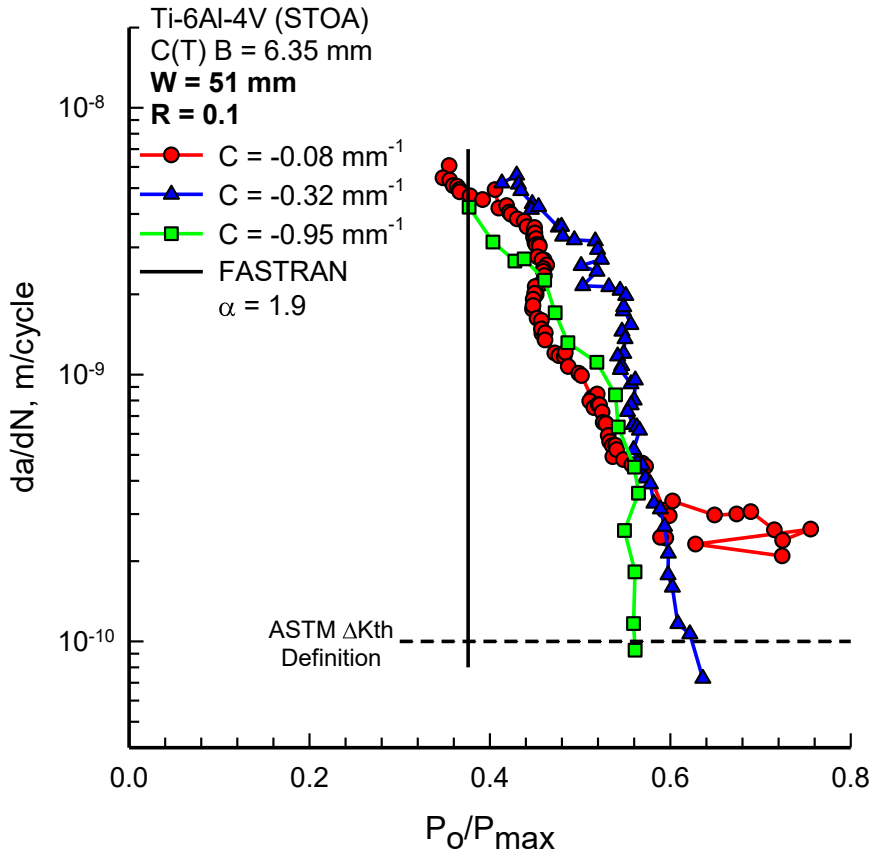

Figure 6.15 Comparison of the OP0 based crack-opening loads at various load-shed rates for the load-shedding test procedures.

In Figure 6.15, the P_o/P_{max} values at the initiation of the LS test (i.e., at about $5E^{-9}$ m/cycle) are equal to or higher than the FASTRAN-based prediction of P_o/P_{max}. As the crack growth rates approach threshold (i.e., 10^{-10} m/cycle), an increase in P_o/P_{max} values can be observed for all Cs. This suggests an increase in various crack-closure mechanisms that affect the crack growth rates. The higher the P_o/P_{max} value at 10^{-10} m/cycle, the greater is the influence of loading-history and crack-closure. Increased influence of crack-closure causes a weakening of crack-tip driving forces, leading to a proportionately higher (and non-conservative) ΔK_{th} values.

For C = -0.08 mm^{-1} the crack growth rates become dormant at about $3E^{-10}$ m/cycle, following which there is a sudden rise in the P_o/P_{max} values (Figure 6.15). The test does not attain threshold fatigue crack growth rates of 10^{-10} m/cycle. The rise in P_o/P_{max} values may be due to an increasing dominance of the RICC and DICC mechanisms, resulting from continued fatigue cycling at similar ΔK-da/dN values. To recap, at 10^{-10} m/cycle, larger load shed rates (i.e., C = -0.95 mm^{-1}) are less influenced by the load-history effects and crack-closure than lower load shed rates (i.e., C = -0.08 or -0.32 mm^{-1}).

6.9 Analyses of crack extension to achieve threshold conditions using the load-shedding procedures

In a LS test procedure, loads are shed (i.e., ΔK-decreases) at every definite increment of crack length, while the crack growth rates approach the threshold value. The higher the C value, the higher is the rate of load shedding, and the sooner the establishment of threshold fatigue crack growth rates. Hence, the amount of crack

extension necessary to achieve threshold fatigue crack growth rates were determined as a function of C values. For this purpose, crack extension was defined as the difference between the crack length at threshold crack growth rate of 10^{-10} m/cycle and the initial crack length at the beginning of the LS test procedure. The observed crack extensions (linear scale) at various |C| values (log scale) during the LS tests on 51 and 76 mm wide C(T) specimens at R = 0.1 are presented in Figure 6.16.

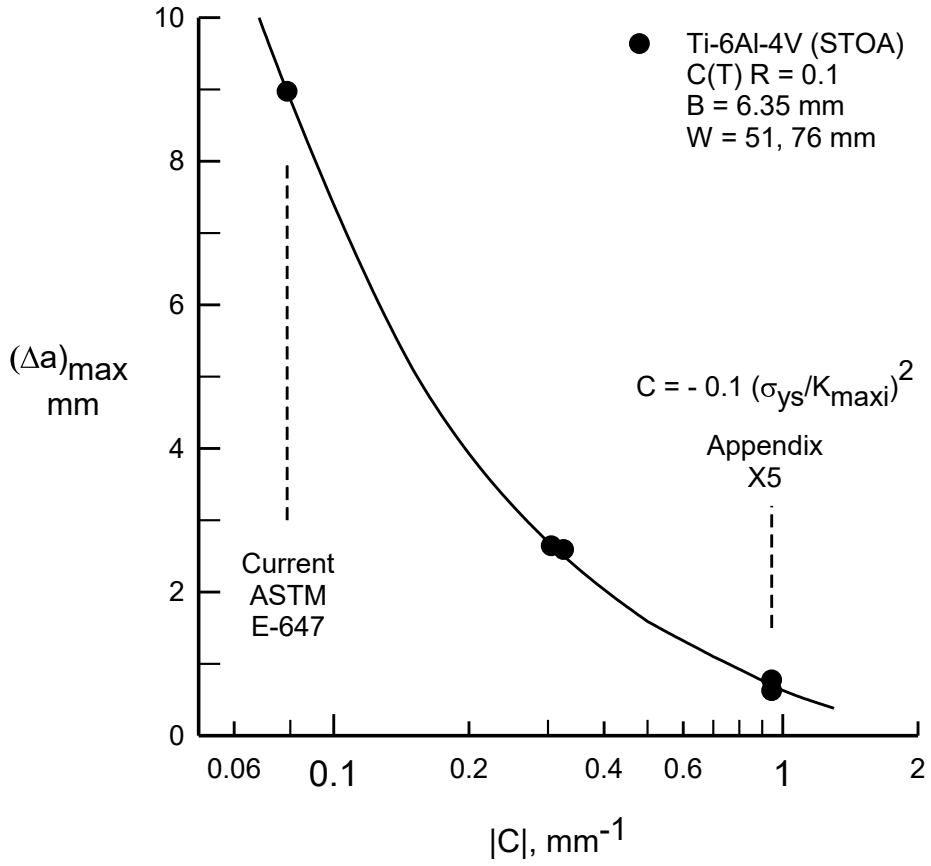

Figure 6.16 Crack extension to achieve threshold conditions at various C values using the proposed load-shedding test procedures.

A test procedure to determine the threshold fatigue crack growth rates must consider an adequate specimen size, material volume, and crack growth to account for various metallurgical features. In Figure 6.16, the crack extension (i.e., amount of material length investigated) to achieve threshold conditions is the highest for the lowest |C| value of 0.08 mm^{-1}. As the |C| values increase, the length of crack extension to achieve threshold decreases. A summary of crack extension to achieve threshold crack growth rate at various C values during the LS tests are presented in Table 6.2.

Table 6.2 Summary of crack extension to achieve threshold crack growth rates at various C values during the load-shedding test procedures on C(T) at R = 0.1.

Specimen Width	Normalized K-gradient, C	Crack Extension
51 mm	-0.08 mm^{-1}	8.9713 mm
	-0.32 mm^{-1}	2.5895 mm
	-0.95 mm^{-1}	0.7722 mm
76 mm	-0.32 mm^{-1}	2.6416 mm
	-0.95 mm^{-1}	0.6226 mm

CHAPTER VII

CONCLUSIONS

The fatigue crack growth rate behavior in the threshold and near-threshold regimes for a Ti-6Al-4V (STOA) alloy was studied using the two proposed ASTM procedures- (1) load-shedding (LS) using a larger load-shed rate than the current ASTM load-reduction (LR) test procedure, and (2) compression pre-cracking constant-amplitude (CPCA) or load-increasing (CPLI) and load-shedding (CPLS). Threshold fatigue crack growth rates were generated at a low stress ratio (R = 0.1) on compact C(T) specimens of two different widths (W = 51 and 76 mm). These test data were compared to previous test data [27, 32] produced from the same batch of material using the current LR and the CPCA procedures.

All the test employing decreasing ΔK or K values (i.e. LR, LS, and CPLS test procedures) were influenced by prior loading-history and various crack-closure mechanisms, leading to higher (potentially non-conservative) thresholds values (ΔK_{th}) and slower crack growths in the threshold regime. As the crack growth rates approach threshold (at 10^{-10} m/cycle), a rise in crack-opening loads was observed in all low load ratio (R = 0.1) LS test procedures. The magnitude of crack-opening loads, which indicate the inherent influence of loading-history and crack-closure, was the

highest at threshold for the LS test with normalized K-gradient (C) value of -0.08 mm^{-1}.

At low R, no test procedure provided an exact representation of the ΔK_{th} value or the fatigue crack growth rates in the threshold regime. The LS tests (tests at C values of -0.08, -0.32, and -0.95 mm^{-1}) produced similar crack growth rates. These LS tests generated a ΔK_{th} values that were 15% to 32% higher than the estimated threshold stress-intensity factor range $(\Delta^* K_{th})_{R=0.1}$. The compression pre-cracking (CP) test procedures were a *significant* improvement over LR or LS test procedures. Hence, the CPLS test procedure is a more accurate alternative for developing low crack growth rates in the threshold regime. The CPLS test procedure produced a ΔK_{th} value that was 10% higher than $(\Delta^* K_{th})_{R=0.1.}$ Further research is required for developing test procedure(s) capable of providing a more definitive representation of the ΔK_{th} value and closure-free fatigue crack growth rates in the threshold regime.

Additionally, it was observed that both LR and LS procedures produced different ΔK_{th} values that depended on specimen width; wider 76 mm specimens produced higher ΔK_{th} and lower fatigue crack growth rates in comparison to narrower 51 mm specimens for the same R values (R = 0.1 or 0.4). The effect of specimen width observed in the LR and LS test procedures is a violation of certain fracture mechanics concepts, where crack growth rate behavior can be correlated with the alternating stress-intensity factor range (ΔK) for a given R. In contrast, the more robust CP test procedures produced consistent crack growth rates over the same range of ΔK values examined, independent of the specimen width.

Based on this study, it is recommended that the proposed LS procedure be rejected in favor of the LR test procedure. The LR test, however, should be restricted to $R \geq 0.7$ tests. Further, it is recommended to use the CPCA and/or CPLI test procedures for generating near-threshold fatigue crack growth rates, and the CPLS for generating threshold fatigue crack growth rates, for all $R \geq 0.1$.

REFERENCES

[1] Irwin, G. R. (1957). Analysis of Stresses and Strains Near the End of a Crack Traversing a Plate. Journal of Applied Mechanics, 24, 361-364.

[2] Paris, P. C., Gomez, M. & Anderson, W. E. (1961). A Rational Analytic Theory of Fatigue. The Trends in Engineering, (13). 9-14.

[3] Paris, P. C. & Erdogan, F. (1963). A Critical Analysis of Crack Propagation Laws. Journal of Basic Engineering, 85(4), 528-534.

[4] Frost, N. E. (1966). The Growth of Fatigue Cracks. First International Conference on Fracture. Sendai, Japan.

[5] Bucci, R. J. (1981). Development of A Proposed ASTM Standard Test Method for Near-Threshold Fatigue Crack Growth Rate Measurement. In Hudak, S. J., & Bucci, R. J. (Eds.), Fatigue Crack Growth Measurement and Data Analysis, ASTM STP 738. West Conshohocken, PA: ASTM International. pp. 5-28.

[6] Barsom, J. M. (1971). Fatigue Crack Propagation in Steels of Various Yield Strengths. Journal of Engineering for Industry, 93(4), 1190-1196.

[7] Damage Tolerance and Fatigue Evaluation of Structure. Title 14 Code of Federal Regulations, Part 25, Section 571. Federal Aviation Regulations.

[8] Boyce, B., & Ritchie, R. (2001). Effect of Load Ratio and Maximum Stress Intensity on the Fatigue Threshold in Ti–6Al–4V. Engineering Fracture Mechanics, 68(2), 129-147.

[9] Elber, W. (1970). Fatigue Crack Closure Under Cyclic Tension. Engineering Fracture Mechanics, 2(1), 37-45.

[10] Elber, W. (1971). The Significance of Fatigue Crack Closure. In Rosenfeld, M. (Ed.), Damage Tolerance in Aircraft Structures, ASTM STP 486. West Conshohocken, PA: ASTM International. pp. 230-242.

[11] Newman Jr., J. C. (1983). A Nonlinear Fracture Mechanics Approach to the Growth of Small Cracks. Behavior of Short Cracks in Airframe Components, AGARD CP-328, 6.1-6.27.

[12] McEvily, A. J. (1988). On Crack Closure in Fatigue Crack Growth. In Newman Jr., J. (Ed.), Mechanics of Fatigue Crack Closure, ASTM STP 982. West Conshohocken, PA: ASTM International. pp. 35-43.

[13] Ward-Close, C. M., & Ritchie, R. O. (1988). On the Role of Crack Closure Mechanisms in Influencing Fatigue Crack Growth Following Tensile Overloads in a Titanium Alloy: Near-threshold Versus Higher ΔK Behavior. In Newman Jr., J. (Ed.), Mechanics of Fatigue Crack Closure, ASTM STP 982. West Conshohocken, PA: ASTM International. pp. 93-111.

[14] Paris, P. C., Bucci, R. J., Wessel, E. T., Clark, W. G., & Mager, T. R. (1972). Extensive Study of Low Fatigue Crack Growth Rates in A533 and A508 Steels. In Corten, H. & Gallagher, J. (Eds.), Stress Analysis and Growth of Cracks: Proceedings of the 1971 National Symposium on Fracture Mechanics: Part 1, ASTM STP 513. West Conshohocken, PA: ASTM International. pp. 141-176.

[15] Purushothaman, S., & Tien, J. K. (1975). A Fatigue Crack Growth Mechanism for Ductile Materials. Scripta Metallurgica, 9, 923-926.

[16] Suresh, S., Zamiski, G. F., & Ritchie, R. O. (1981). Oxide Induced Crack Closure: An Explanation for Near-Threshold Corrosion Fatigue Crack Growth Behavior. Metallurgical Transactions, 12A, 1435-1443.

[17] Suresh, S., & Ritchie, R. O. (1982). A Geometric Model for Fatigue Crack Closure Induced by Surface Roughness. Metallurgical Transactions, 13A, 1627-1631.

[18] Walker, N., & Beevers, C. J. (1979). A Fatigue Crack Closure Mechanism in Titanium. Fatigue & Fracture of Engineering Materials & Structures, 1(1), 135-148.

[19] Newman Jr., J. C. (2000). Analyses of Fatigue Crack Growth and Closure near-threshold Conditions for Large-Crack Behavior. In Newman Jr., J., & Piascik, R. S. (Eds.), Fatigue Crack Growth Thresholds, Endurance Limits, and Design, ASTM STP 1372. West Conshohocken, PA: ASTM International. pp. 227-251.

[20] McClung, R. C. (2000). Analyses of Fatigue Crack Closure During Simulated Threshold Testing. In Newman Jr., J., & Piascik, R. S. (Eds.), Fatigue Crack Growth Thresholds, Endurance Limits, and Design, ASTM STP 1372. West Conshohocken, PA: ASTM International. pp. 227-251.

[21] Jackson, P., Wallbrink, C., Walker, K., Mongru, D., & Hu, W. (2011). Exploration of Questions Regarding Modelling of Crack Growth Behaviour Under Practical Combinations of Aircraft Spectra, Stress Levels and Materials. Victoria, Australia: Defence Science and Technology Organisation, Air Vehicles Division.

[22] Standard Test Method for Measurement of Fatigue Crack Growth Rates. (2015). ASTM E647-15e1. West Conshohocken, PA: ASTM International.

[23] Forth, S. C., Newman Jr, J. C., & Forman, R. G. (2003). On Generating Fatigue Crack Growth Thresholds. International Journal of Fatigue, 25(1), 9-15.

[24] Newman Jr., J., Schneider, J., Daniel, A., & McKnight, D. (2005). Compression Pre-Cracking to Generate Near-threshold Fatigue crack growth Rates in Two Aluminum Alloys. International Journal of Fatigue, 27(10-12), 1432-1440.

[25] Forth, S. C., Newman Jr., J. C., & Forman, R. G. (2005). Evaluation of Fatigue Crack Thresholds Using Various Experimental Methods. Journal of ASTM International, 2(6), 1-16.

[26] Yamada, Y., & Newman Jr., J. C. (2008). Elastic-Plastic Finite-Element Analyses of Compression Pre-cracking and Its Influence on Subsequent Fatigue crack Growth. Journal ASTM International, 5(8), 1-13.

[27] Ruschau, J. J., & Newman Jr., J. C. (2008). Compression Pre-cracking to Generate Near-threshold Fatigue crack growth Rates in an Aluminum and Titanium Alloy. Journal of ASTM International, 5(7), 1-11.

[28] Yamada, Y., & Newman Jr, J. C. (2009). Crack Closure Under High Load-Ratio Conditions for Inconel 718 near-threshold Behavior. Engineering Fracture Mechanics, 76(2), 209-220.

[29] Yamada, Y., & Newman Jr., J. C. (2009). Crack Closure Behavior of 2324-T39 Aluminum Alloy near-threshold Conditions for High Load Ratio and Constant K_{max} Tests. International Journal of Fatigue, 31(11-12), 1780-1787.

[30] Newman Jr., J. C., & Yamada, Y (2010). Crack-Closure Behavior of 7050 Aluminum Alloy near-threshold Conditions for Wide Range in Load Ratios and Constant K_{max} Tests. Journal of ASTM International, 7(4), 1-16.

[31] Newman Jr., J. C., & Yamada, Y. (2010). Compression Pre-Cracking Methods to Generate Near-Threshold Fatigue Crack Growth Rate Data. International Journal of Fatigue, 32(6), 879-885.

[32] Newman Jr., J. C., Ruschau, J. J., & Hill, M. R. (2011). Improved Test Method for Very Low Fatigue Crack Growth Rate Data. Fatigue and Fracture Engineering Materials and Structures, 34(4), 270-279.

[33] Schmidt, R. A., & Paris, P. C. (1973). Threshold for Fatigue Crack Propagation and the Effects of Load Ratio and Frequency. In Kaufman, J., Swedlow, J., Corten, H., Srawley, J., Heyer, R., Wessel, E., and Irwin, G. (Eds.), Progress in Flaw Growth and Fracture Toughness Testing, ASTM STP 536. West Conshohocken, PA: ASTM International. pp. 79-94.

[34] Hudak Jr, S. J., Saxena, A., Bucci, R. J., & Malcolm, R. C. (1978). Development of Standard Methods of Testing and Analyzing Fatigue Crack Growth Rate Data. Pittsburgh, PA: Westinghouse Research and Development Center.

[35] Minakawa, K., Newman Jr., J. C., & McEvily, A. J. (1983). A Critical Study of the Closure Effect on Near-Threshold Fatigue Crack Growth. Fatigue and Fracture of Engineering Materials and Structures, 6(4), 359-365.

[36] Herman, W. A., Hertzberg, R. W., & Jaccard, R. (1988). A Simplified Laboratory Approach for the Prediction of Short Crack Behavior in Engineering Structures. Fatigue of Engineering Materials and Structures, 11(4), 303-320.

[37] Smith, S. W., & Piascik, R. S. (2000). An Indirect Technique for Determining Closure-Free Fatigue Crack Growth Behavior. In Newman Jr., J., & Piascik, R. S. (Eds.), Fatigue Crack Growth Thresholds, Endurance Limits, and Design, ASTM STP 1372. West Conshohocken, PA: ASTM International. pp. 109-122.

[38] Yamada, Y., & Newman Jr., J. C. (2010). Crack Closure Under High Load Ratio and K_{max} Test Conditions. Procedia Engineering, 2(1), 71-82.

[39] Suresh, S. (1985). Crack Initiation in Cyclic Compression and its Application. Engineering Fracture Mechanics, 21(3), 453-463.

[40] Pippan, R. (1987). The Growth of Short Cracks Under Cyclic Compression. Fatigue & Fracture of Engineering Materials & Structures, 9(5), 319-328.

[41] Pippan, R., Plöchl, L., Klanner, F., & Stüwe, H. P. (1994). The Use of Fatigue Specimens Pre-Cracked In Compression for Measuring Threshold Values And Crack Growth. Journal of Testing and Evaluation, 22(2), 98-103.

[42] Schindler, H. J., Cheng, W., & Finnie, I. (1997). Experimental Determination of Stress Intensity Factors due to Residual Stresses. Experimental Mechanics, 37(3), 272-277.

[43] Donald, J. K. (1988). A Procedure for Standardizing Crack Closure Levels. In Newman Jr., J. (Ed.), Mechanics of Fatigue Crack Closure, ASTM STP 982. West Conshohocken, PA: ASTM International. pp. 222-229.

[44] Elber, W. (1975). Crack Closure and Crack Growth Measurements in Surface-Flawed Titanium Alloy Ti-6Al-4V. NASA-TN-D-8010. NASA Langley Research Center. Hampton, VA.

[45] Garr, K. R., & Hresko, G. C. (2000). A Size Effect on the Fatigue Crack Growth Rate Threshold of Alloy 718. In Newman Jr., J., & Piascik, R. S. (Eds.), Fatigue Crack Growth Thresholds, Endurance Limits, and Design, , ASTM STP 1372. West Conshohocken, PA: ASTM International. pp. 155-174.

[46] Newman Jr., J. C. (1992). FASTRAN II- A Fatigue Crack Growth Structural Analysis Program. NASA Langley Research Center. Hampton, VA.